Limits to the critical current in high-T_c superconducting tapes

L. N. Bulaevskii, L. L. Daemen, M. P. Maley, and J. Y. Coulter
Superconductivity Technology Center, Los Alamos National Laboratory, Los Alamos, New Mexico 87545
(Received 23 February 1993)

Within the framework of the "brick-wall" model, we review in detail how various physical mechanisms could act to limit the critical current in high-T_c superconducting tapes. The brick-wall model attempts to mimic in a simplified manner the complicated tape microstructure. We generalized it to take into account a distribution of grains sizes and possible different strengths of weak links between the grains and the existence of weak links associated with intergrain boundaries perpendicular to the plane of the tape. We discuss what experiments can distinguish between a situation where weak links limit the critical current, and another plausible scenario where intragranular pinning is the limiting factor. Our conclusion is that according to the available experimental data only a small, well-connected fraction of the high-J_c tapes is effective in providing high critical current densities. For this fraction of the tape, pinning turns out to be the limiting mechanism. Finally, several possibilities for increasing the critical current of the high-T_c superconducting tapes are discussed.

I. INTRODUCTION

Recent developments in the processing of tape conductors based upon the bismuth high-temperature superconducting (HTS) compounds have shown great promise in reducing "weak link" effects and in achieving high-transport critical current densities. It is now a well-established fact that the microstructure of these superconducting tapes[1] consists of small platelets with large aspect ratios. These platelets have their c axis perpendicular to the plane determined by the largest dimensions of the grain. They are oriented so that their c axes are aligned almost perfectly and are perpendicular to the plane of the tape. The a and b axes are usually oriented at random from platelet to platelet. Because of this particular microstructure, at least two types of grain boundaries exist in a tape: c axis grain boundaries in which the junction plane is parallel to the ab planes and a or b axis grain boundaries for which the junction plane is perpendicular to the ab planes. From the point of view of current transport these grain boundaries form weak links, and it is therefore important to address the question of whether these weak links limit the critical current of the tape or whether the intragranular current is the bottleneck for current transport.

Our main goal in this article is to review briefly what is known experimentally about the microstructure of the Bi-based high-T_c superconducting tapes, their I-V curves, and the field and temperature dependence of the critical current. Within the framework of brick-wall model, we discuss which mechanisms limit the critical current in these tapes.

In Sec. II we give a brief overview of the microstructural properties of superconducting tapes and point out what microstructural features are likely to be important for current transport.

In Sec. III we describe in some detail "brick-wall" model.[2,3] This simple model attempts to describe the gross features of the microstructure of a tape. It assumes that the tape is made of "bricks" (grains) of equal lengths stacked in a brick-wall manner. The main idea of the model is that in order to flow along the tape, the current follows a complicated path, weaving through a series of large-area c axis twist boundaries, bypassing the small-area a and b axis tilt boundaries in the direct path of the current. The bottleneck for current transport is supposedly the critical current across the Josephson junctions (or weak links) corresponding to the c axis grain boundaries. Intragranular pinning is assumed to be so strong that it does not limit the critical current. In this approach the direct current through the a and b axis tilt boundaries is assumed to be small compared to the corresponding current along the c axis.

We generalize the brick-wall model by considering the possibility that the current might flow across weak links formed by the a and b axis grain boundaries. We then consider the more complex situation where the bricks may have quite different lengths.

In Sec. IV we consider the experimental data which characterize the limitations on the critical current imposed by the intragranular pinning mechanism.

In Secs. V and VI we consider theoretically the dependence of the critical current on magnetic field and temperature in c axis and a and b axis weak links.

In Sec. VII we summarize the experimental results currently available for I-V curves and the field and temperature dependence of the critical current in high-T_c superconducting tapes (irradiated and unirradiated). Based on the current-limiting mechanisms discussed in the previous sections and experimental data, we examine different scenarios from current transport dominated exclusively by the presence of weak links, to current transport dominated by intragranular pinning.

Finally, in Sec. VIII we point out which parameters should be optimized to increase the critical current of the high-T_c superconducting tapes.

0163-1829/93/48(18)/13798(19)/$06.00

II. SUPERCONDUCTING TAPE MICROSTRUCTURE

It is impossible at this point in time to determine with complete certainty those aspects of the tapes and films microstructure that have a significant impact on their current-carrying properties. However, a number of microstructural features have been identified that appear to have a beneficial effect on the critical current whereas others seem to be undesirable.[4–6]

The microstructure of superconducting tapes and films of the high-T_c materials varies greatly from sample to sample depending on composition as well as chemical, thermal, and mechanical processing. However, most of the high-J_c tapes seem to have the following characteristics in common.

The main structural units of the tapes are highly aligned platelet-shaped grains. The aspect ratio of the grains varies depending on the processing steps to which the tape was subjected, but the grains are typically larger in the *ab* plane than along the *c* axis with typical length (L) to thickness (D) ratios $\simeq 20$ deep inside the tapes, and presumably larger near the silver cladding (see below). Their *ab* planes grow predominantly parallel to the Ag cladding. The grain *c* axes are almost parallel, leading to a highly textured microstructure; see Fig. 1. Inside a tape, a typical grain length is $L \simeq 20$ μm.

There appear to be essentially two types of grain boundaries: *c* axis grain boundaries and *a* and *b* axis grain boundaries. The twist boundaries (*c* axis boundaries) arise when two grains are stacked on top of each other with their *c* axes parallel. The chemical bonding and electron transfer across these boundaries are depressed in comparison with the coupling of the layers inside the grains. This is because of the twist and larger separation of the layers forming the boundary. Upon taking into account that the interlayer coupling inside the grains for $Bi_2Sr_2CaCu_2O_8$ (Bi 2:2:1:2) and $Bi_2Sr_2Ca_2Cu_3O_{10}$ (Bi 2:2:2:3) has the Josephson character[7] it seems reasonable to conclude that the *c* axis intergrain boundaries are weak links. A schematic representation of the layer arrangement is given in Fig. 2(a). The orientation of the *a* and *b* axes in a grain varies at random from one grain to the next. The *a* and *b* axis grain boundaries correspond to the interface between two adjacent grains. They are typically less well defined than

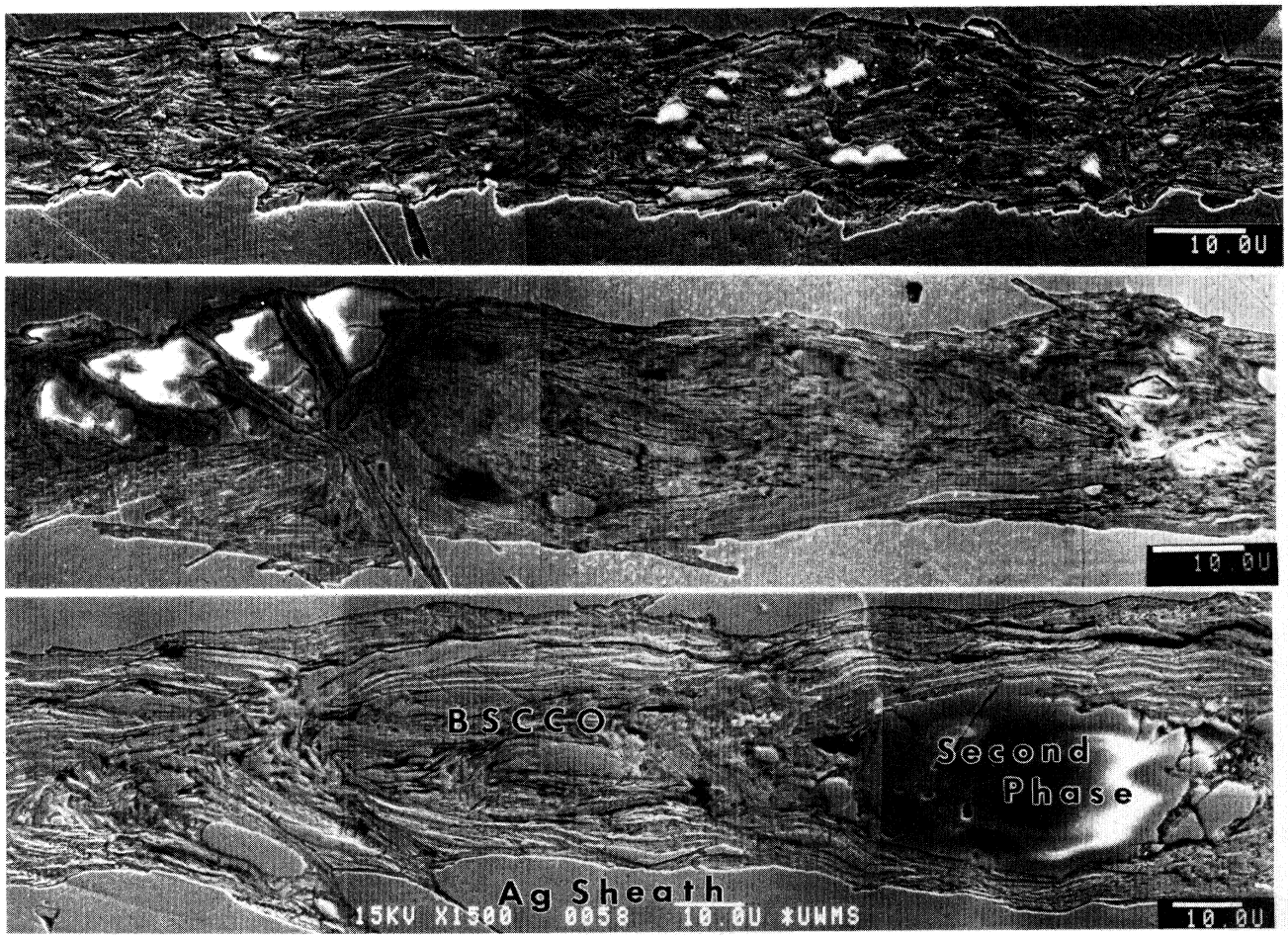

FIG. 1. Scanning electron microscope (SEM) micrographs of polished and etched thin-longitudinal cross-section samples: (a) solid state, (b) fast-cooled, and (c) slow cooled. The local grain alignment interrupted by second-phase particles can be seen clearly (courtesy Yvonne High, Ref. 4).

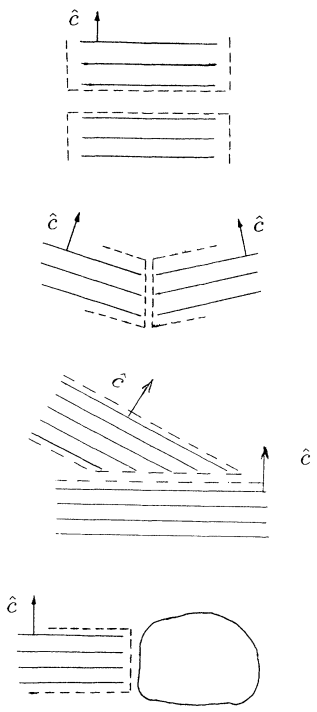

FIG. 2. Schematic representation of different intergrain boundaries. (a) c axis grain boundary, (b) a and b axis grain boundary, (c) colony boundary, (d) grain secondary-phase boundary.

the c axis grain boundaries. The layers are disrupted here mostly because of the tilting of the layers which depresses strongly the electron transfer across the boundary.[8] A schematic representation of the layers near an a and b axis boundary is shown in Fig. 2(b).

A second characteristic feature of the tapes is the existence of large regions in the material where the c axes of the grains are very well aligned ("colonies").[4] A colony boundary is formed when two colonies with significantly different c axis orientations collide with each other; see Fig. 3. A schematic representation of the layers arrangement at a colony boundary is shown in Fig. 2(c). Hensel *et al.*[6] found little or no evidence for the presence of second phase in the contact region along colony boundaries. For this reason, they assumed that colony boundaries, i.e., slightly misaligned c axis boundaries, provide quite good connection of the grains, and current can flow along the ab planes through colony boundaries better than through neighboring grains. If such assumption is correct, it means that the *effective* length of the grains for electron transport is larger along such boundaries.

Third, near the Ag-superconductor interface the grains are almost perfectly aligned with the Ag and this alignment extends over long distances; see Fig. 4. These grains and their almost perfect alignment are interrupted by the grains that are tilted with respect to the silver surface. Nevertheless, it seems reasonable to assume that despite these interruptions, the a and b axis grain boundaries are less pronounced for the grains near the silver so that electron transfer near that interface should be better than inside the tape. This means that the grains are probably more tightly coupled at an a and b axis grain boundary near the Ag interface and therefore the *effective* length of the grains for electron transport near the silver surface may be much larger than inside the tape. Notice that this feature is commonly observed but does not seem to be a universal feature of all Bi-Sr-Ca-Cu-O (BSCCO) superconducting tapes. A polished Bi 2:2:2:3 tape seen in optical reflection is shown in Fig. 5. It has a more or less homogeneous distribution of grain lengths. The same distribution has been seen also by Hensel *et al.*[6]

FIG. 3. Transmission electron microscope (TEM) micrography of a thin-longitudinal cross section of a fast-cooled sample showing an overview of the grain morphology and grain boundaries (beam direction perpendicular to the c axis of Bi 2:2:1:2). The colony boundaries are indicated (courtesy Yi Feng, Ref. 4).

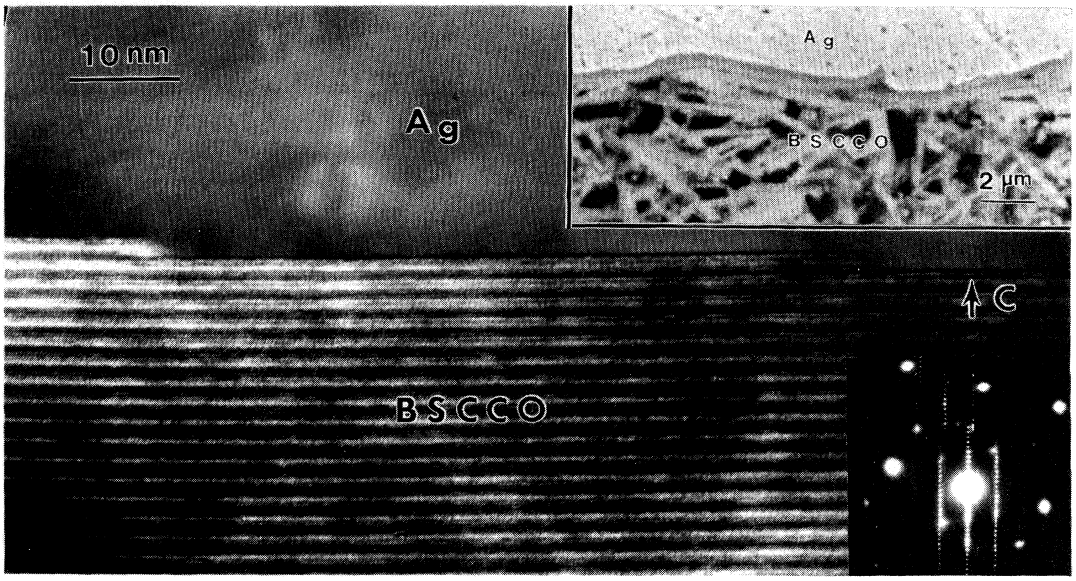

FIG. 4. TEM (001) lattice fringe image of the Bi 2:2:1:2 phase in the slow-cooled sample showing its c axis perpendicular to the interface with the Ag cladding. The inset is a SEM micrography of a transverse cross section of the same tape (courtesy Yi Feng, Ref. 5).

Various defects can also be present in the tapes. First, secondary phases are usually present; see Fig. 1. For example, amorphous phases have often been observed inside the tapes, and large grains of nonsuperconducting materials or incompletely reacted phases are commonly observed. Their main effect on the microstructure is to cause a major disruption of the alignment of the superconducting grains: The layer arrangement near a secondary phase boundary is shown schematically in Fig. 2(d). The superconducting layers are terminated there. Some fraction of the Bi 2:2:1:2 phase with lower T_c is present in Bi 2:2:2:3 tapes due to the incomplete chemical transformation of the original Bi 2:2:1:2 phase into the final Bi 2:2:2:3 phase. The remaining Bi 2:2:1:2 layers form predominantly near c axis twist boundaries.[9] They weaken the intergrain coupling across such boundaries.

Second, various defects such as stacking faults, grain intergrowths, and other more complex defects have been reported. Their effect on the current-carrying properties is unclear at this point. Finally, cracks, voids, and other large scale defects have usually a disastrous effect on the critical current.

It is worth mentioning that films seem to have a microstructure very similar to that of the superconducting tapes. Because of the greater ease with which the deposition conditions can be controlled, films have consistently better microstructural characteristics and larger critical currents than tapes. Crudely speaking, low-quality films behave more like tapes, whereas higher-quality films exhibit characteristics closer to that of a single crystal. So, although we use mostly the superconducting tapes terminology in what follows, it should be kept in mind that most of our results apply to films as well.

III. CRITICAL CURRENT IN THE "BRICK-WALL" MODEL

We use the brick-wall model to describe in a more quantitative way the behavior of the critical current, taking into account the microstructure of the tapes. The original brick-wall model[2,3,10] assumed that the tape was made up of bricks similar in size and shape. In this model the Josephson junctions perpendicular to the c axis [shown in Fig. 2(a)] were assumed to be the bottleneck for current transport. A schematic representation of this model is shown in Fig. 6(a). Here we generalize this model to take into account different grains lengths and allow the current to flow through all possible weak links, Figs. 2(b) and 2(c).

We introduce the following notations.

(i) L is the length of the grains in the a and b directions. Below we consider a situation where only two very different grain lengths are present: L_1 (presumably for the grains deep inside the tape) and $L_2 \gg L_1$ (for the grains near the Ag interface or near the colony boundary); see Fig. 6(b).

(ii) a is the fraction of long bricks; the fraction of short bricks is $(1-a)$.

(iii) D is the average thickness of the grains.

(iv) j_p is the intragrain critical current determined by pinning.

(v) $j_{w,c}$ is the critical current density for the Josephson junctions corresponding to the c axis twist boundaries (which are parallel to the ab plane).

(vi) $j_{w,ab}$ is the critical current density for the Josephson junctions corresponding to a and b axis tilt boundaries (which are perpendicular to the ab plane).

We call such a structure "brick-wall"-like regardless of

what kind of mechanism limits the critical current. The brick-wall model with two lengths is equivalent to the model with strong- and weak-linked grains discussed by Tkaczyk *et al.*[11]

Let us now define j_p and the critical current density of the tape. The tape critical current density can be obtained from transport ($j_{c,t}$) or magnetization ($j_{c,m}$) measurements.[12] $j_{c,t}$ is the current measured when a given small voltage develops across the tape. This voltage is (usually) arbitrarily taken to correspond to an average electric field E_c of about 1 μV/cm. Because of flux creep the current inside the grains produces the electric field $E_p(j) = E_0(j/j_0)^p$ (we will discuss this dependence below). If the current density across weak links does not exceed the critical current ($j_{w,c}$ and $j_{w,ab}$), the critical current of the tape is determined by the condition $E_p(j) = E_c$ and $j_c = j_p = j_0(E_c/E_0)^{1/p}$. If the current across a weak link exceeds the corresponding critical current, an additional electric field across the junction should be taken into account.

Altogether, there are three cases of interest depending on the relative values of the parameters.

(1) If $j_p < j_1, j_2$ where $j_{1,2} = j_{w,ab} + j_{w,c}L_{1,2}/D$, then intragrain pinning limits the critical current, $j_c = j_p$, and the I-V curve is given by the expression

$$E/E_0 = (j/j_0)^p. \tag{3.1}$$

The dependence of the average electric field on the average current density j is a power law; see Fig. 7(a). The weak links are unimportant, and the I-V curve is the same as that of a single crystal or a perfect film. We refer to this case "limitation by pinning."

(2) If $j_1 < j_p$, then for current densities $j < j_1$ the dependence $E(j)$ is given by Eq. (3.1). For $j > j_1$ the current density across the short bricks is j_1. Across the long bricks the current density is larger than j_1. If E reaches E_c before j exceeds j_2, we obtain the dependence $E(j)$:

$$\begin{aligned} E/E_0 &= (j/j_0)^p, & j &< j_1, \\ E/E_0 &= (aj_0)^{-p}[j-(1-a)j_1]^p, & j &> j_1, \end{aligned} \tag{3.2}$$

where we assumed that the long bricks near the silver produce the measured voltage. The dependence given by Eq. (3.2) is shown in Fig. 7(b). The tape critical current density is given by the expression

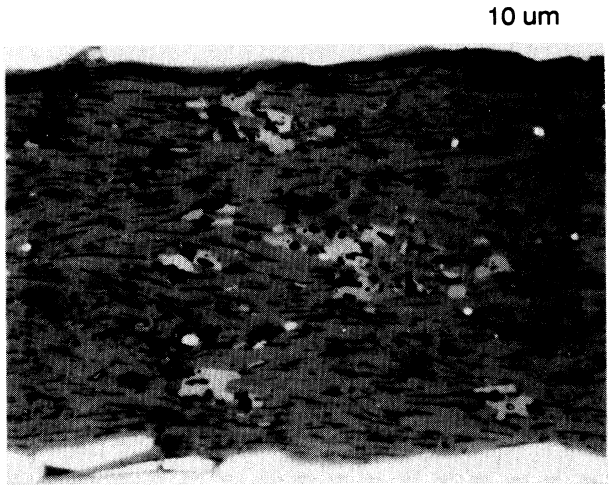

FIG. 5. Optical reflection in polished, rolled, sintered Bi 2:2:2:3 tape. Gray regions are Bi 2:2:2:3 grains, black regions are epaxi, which is used to fill empty space in between grains before polishing, and white regions are secondary phases.

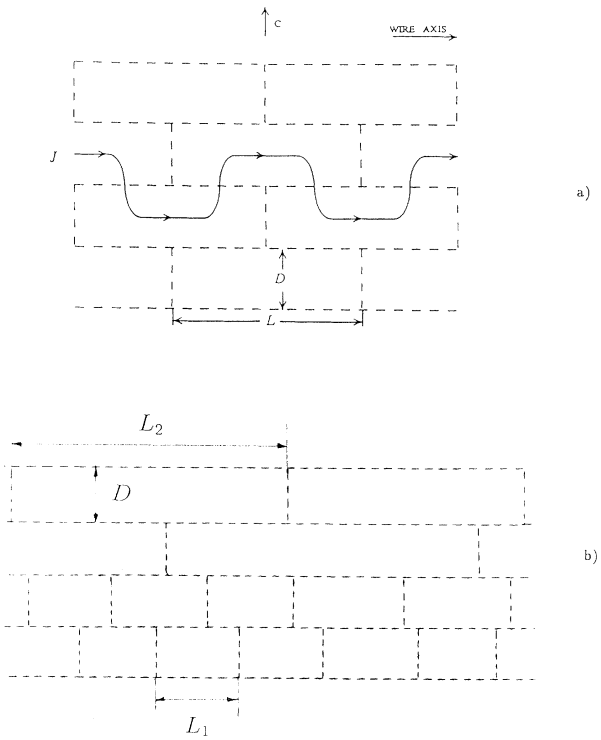

FIG. 6. Schematic representation of the brick-wall model microstructure with (a) similar bricks and (b) with bricks of different lengths.

$$j_c = (1-a)j_1 + aj_p. \tag{3.3}$$

We call this case "partial limitation by weak links."

(3) In the same situation $j_1 < j_p$, if j exceeds j_2 before E reaches E_c, the average electric field increases rapidly for current densities j larger than j_2 due to the presence of a voltage across the junctions. j_c coincides practically with j_2. The I-V curve in this case is shown in Fig. 7(c). This case will be referred to as "limitation by weak links." The original brick-wall model[2,3] corresponds to this case with $j_1 = 0$.

Note that in all cases the extrapolation of the dependence E vs j from small E to E_c gives for the critical current the value j_p.

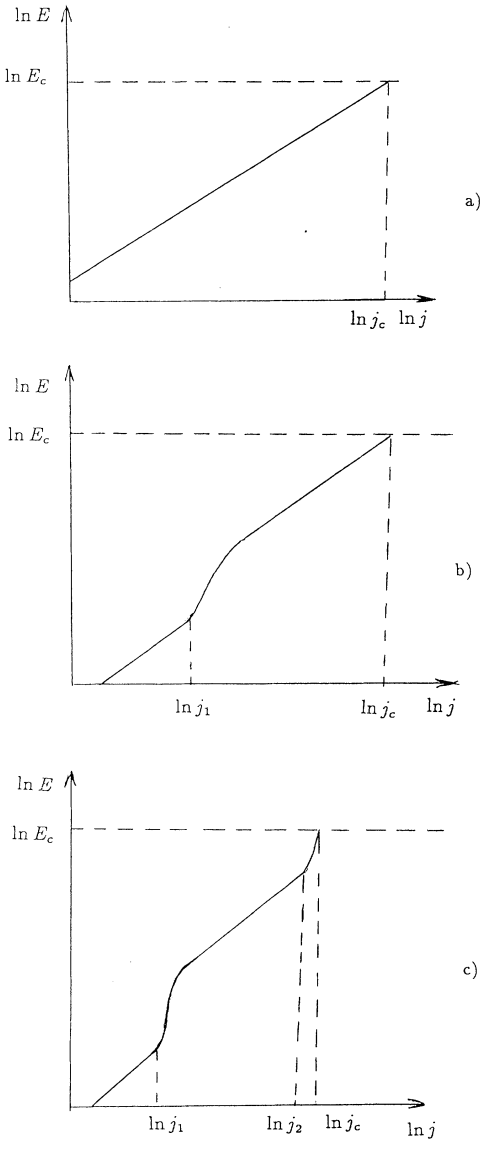

FIG. 7. The I-V curve for tapes (schematically): (a) Current does not exceed the critical current of weak links, (b) current exceeds the critical current of weak links between short bricks, and (c) current exceeds the critical current of weak links in both short and long bricks.

From a practical point of view an interesting situation corresponds to j_1 very small in comparison to aj_p. In that case, only the long bricks contribute significantly for all electric fields except at very small E:

$$E/E_0 = (j/aj_0)^p. \tag{3.4}$$

If E reaches E_c before j exceeds j_2, the critical current is $j_c = aj_p$; otherwise $j_c = j_2$. In the former case, the I-V curve is the same as in the first regime described above, namely, a power law. However, the critical current is now smaller than in the sample without weak links by a factor a. The same result is also valid if practically infinite superconducting paths exist in the tape. The fraction of the effective cross section of these paths is a. All other parts of the sample, regardless of their nature, are not actively participating in current transport in this case: They can be short bricks or nonsuperconducting phases.

In a magnetization measurement, the irreversible component of the magnetization M is studied as a function of applied magnetic field and time. The magnetization critical current density is extracted using Bean's formula $j_{c,m} = 3\Delta M/2cR$, where ΔM is the width of the magnetization loop and R is the average diameter of a cross section of the sample perpendicular to the field. Magnetization measurements are performed typically 10–60 s after applying the external field. During this period, rapid flux creep allows relaxation of the flux profile away from the Bean critical state by an amount that is a function of temperature and field. In typical experiments the decay of the magnetization, dM/dt, produces an electric field at the sample surface of the order of 10^{-10} V/cm. These fields are well below the critical electric field assumed in the definition of the critical current $j_{c,t}$ in the transport measurements. In order to obtain larger values of E the magnetic field must change sufficiently rapidly. Only in this case can E_c be reached. More generally, measurements of the magnetization relaxation $M(t)$ give information on the current j and the electric field $E = (4\pi/cw)(dM/dt)$ where w is the sample thickness. Therefore, in principle, I-V curves could be obtained as a result of these measurements. Note that the third regime cannot be achieved in magnetization measurements because the current across the long bricks cannot exceed j_2 in the quasiequilibrium states studied by magnetization measurements (the quasiequilibrium states being due to the pinning of vortices).

When the same voltage criterion is used, the critical current densities $j_{c,t}$ and $j_{c,m}$ should coincide if intragranular pinning is the limiting factor. In that case ΔM scales with the size of the sample R. If weak links limit the critical current, $j_{c,m}$ is larger than $j_{c,t}$ due to the additional contribution of the intragranular currents j_pL to ΔM. Usually $R \gg L$, and this contribution is small for well-coupled tapes, and again, ΔM scales with the size of the sample R.

For completely decoupled grains (e.g., in powders obtained by grinding a piece of tape) R should be replaced by L, and ΔM does not scale with size of the sample. The critical current obtained from the magnetization ΔM of

such samples gives the intragranular critical current; i.e., the critical current is limited by pinning exclusively, j_p. In order to obtain j_p, additional information such as the grain size is necessary. Usually L is taken to be 20 μm.

We now analyze the dependence of j_p, $j_{w,c}$, and $j_{w,ab}$ on field, temperature, and concentration of pinning centers. In principle, their dependence on field and temperature can be different, and the crossover from one limiting mechanism to another is possible.[11,13–16] We make use of the available experimental data and theoretical results in an attempt to choose between these three cases (limitation by pinning, partial limitation by pinning, limitation by weak links) and provide a global, unified picture of the current limitation process in high-T_c superconducting tapes.

In the following we will discuss mainly the effect of a perpendicular field on the critical current, because, according to the experimental data, its effect is much more dramatic than the effect of parallel field.[17] When the magnetic field is oriented parallel to the tape, the behavior of the critical current is qualitatively similar to that observed for the perpendicular orientation, but the decrease of the critical current with magnetic field or temperature is much less pronounced. For temperatures larger than 30 K the effect of the parallel field can be easily accounted for. Because of the misalignment of the grains in the tape, every grain is subjected to a small magnetic field directed along its c axis. All the experimental data for moderate and high temperatures can be well described if we realize that this small perpendicular component reduces the critical current more effectively than the component of the applied field parallel to ab plane; see Appendix A and Refs. 6, 18, and 19. Thus measurements of the magnetic field dependence of j_c in parallel fields at moderate and high temperatures do not provide additional information about the mechanism limiting the critical current. However, they provide a useful measure of the degree of grain misalignment.

IV. INTRAGRANULAR PINNING MECHANISM

Information on j_p can be obtained from measurements of the critical current in single crystals or high-quality films where weak links are absent or play a minor role, and from magnetization critical current measurements in powders obtained from grinding a tape.

According to the experimental results for single crystals, high-quality films, and untextured polycrystalline samples (before or after irradiation), the dependence of j_p on field B along c axis (in the interval $0 < B < 10$ T) at moderate and high temperatures (above 15 K) is exponential:[11,20,21]

$$j_p(B,T) = j_p(0,T)\exp[-B/B_p(T)] , \tag{4.1}$$

where B_p depends strongly on T as well as on the concentration and type of defects. The origin of this dependence in a quite broad interval of magnetic field and temperature was unknown up to now. (Notice that in some limiting cases this dependence was obtained theoretically in the collective pinning model; see Refs. 22 and 23.) For thermally activated flux creep this dependence corresponds to the following dependence of the activation energy U on j and B:[24–27]

$$U(B,T,j) = \frac{F(T)}{B}\ln\frac{j_0}{j} , \tag{4.2}$$

and the interaction of vortices is important to obtain this dependence. The flux creep electric field is given as

$$E = E_0\exp\left(-\frac{U}{T}\right) = E_0\left(\frac{j}{j_0}\right)^p , \quad p = \frac{F(T)}{BT} . \tag{4.3}$$

This expression describes the I-V curve in a Bi 2:2:1:2 thin film at $B = 0.1$ T and temperatures 20, 30, 40 K in the range $E = 10^{-13}$–10^{-5} V/cm (magnetization measurements have been performed at low E and transport measurements at large E).[28] After combining this expression with a fixed electric field threshold E_c we get for j_p

$$j_p(B,T) = j_p(0,T)\exp\left[-B\frac{T}{F(T)}\ln\left(\frac{E_0}{E_c}\right)\right] . \tag{4.4}$$

The dependence of j_p on B should become weaker as $B \to 0$ (in the single vortex pinning regime), but so far no information about the dependence of j_c on B in this region is available because of the high values of the critical current and the correspondingly large self-field.

We note that at large current densities (e.g., at low temperatures) a substantial amount of transport current flows through the tape and generates a magnetic field (the so-called self-field) in addition to the applied field. This self-field, if it exceeds the lower critical field at the sample surface, can nucleate vortices inside the sample. Those vortices can in turn contribute to a decrease of the critical current. Hence, this effect should be taken into account when interpreting transport critical current measurements at large current densities (especially at low applied magnetic fields; for more details see Ref. 29 and Appendix B). Notice also that self-field effects depend on the sample shape and dimensions.

Evidently, the critical current determined by pinning should increase as the concentration of pinning centers increases. This is in agreement with the experimental observations of the effect of irradiation in single crystals and untextured polycrystalline samples.[20,30–32] Two types of irradiation defects should be considered. Irradiation by neutrons, protons, or high-energy light ions produces point defects distributed at random throughout the material. These defects vary in size but are typically quite small compared to the coherence length. Irradiation by high-energy heavy ions produces continuous cylindrical tracks (columns) about 5–10 nm in diameter (in the following we discuss the effect of columns parallel to c axis). Inside these columns the superconducting phase is destroyed. For single crystals and untextured polycrystalline samples the behavior of the critical current after irradiation can be characterized as follows.

(1) Both types of irradiation increase the critical current of single crystals and polycrystalline samples of Bi 2:2:1:2 as well as in Tl 2:2:2:3 thin films at all fields and temperatures. This is evidence in favor of a conventional pinning mechanism for the critical current in these sys-

tems. The behavior of the critical current in single crystal Bi 2:2:1:2 after irradiation is shown in Fig. 8. The enhancement of the critical current is quite significant. This is to be expected because a single crystal has intrinsically a low density of defects and consequently pinning is usually weak and can be easily enhanced by irradiation.

(2) The I-V characteristic of Bi 2:2:1:2 thin films obtained by Kummeth *et al.*[33] shows increase of the parameter p, i.e., enhancement of pinning characterized by the value $F(T)$; see Fig. 9.

(3) The maximum activation energy for the depinning of a single vortex in the presence of columnar defects can be obtained from flux creep measurements in Bi 2:2:1:2 single crystals and was found to be of the order of 70 meV. This is only twice as large as the activation energy of untextured polycrystalline bulk samples.[20] In Tl 2:2:2:3 thin films the activation energy increases from 45 meV in unirradiated films up to 95 meV at $\phi_t = 4 \times 10^{11}$ cm^{-2}.[32] This implies that the strongest pinning centers provide an activation energy which is only twice as large as the defects which are introduced naturally during the sample fabrication process. This fact was explained in Ref. 20 by the two-dimensional (2D) nature of the vortices in the highly anisotropic Bi compounds. The point-like nature of the pancake vortices[34] results in very small core pinning energies.[35,36]

The important point is that the value of the critical current in the best thin films of Bi 2:2:1:2 (Ref. 21) and Bi 2:2:2:3 (Ref. 37) at small magnetic fields is about two orders of magnitude larger than in tapes.[12] Note that in tapes pinning is much stronger because of the defects inside the grains produced during the melting phase of the fabrication process. (These defects are mainly dislocations with concentrations of about 10^{10} cm^{-2} and stacking faults; they act as effective pinning centers.[13]) This seems to imply that weak links or nonsuperconducting phases limit the critical current in superconducting tapes; i.e., either "partial limitation by weak links" or "limitation by weak links" is realized.

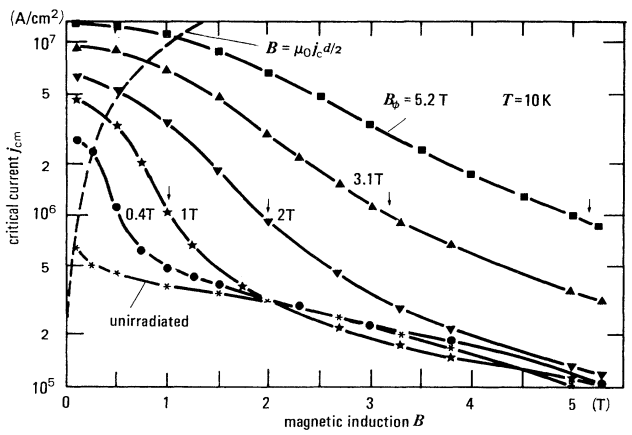

FIG. 8. $j_{c,m}$ is shown as a function of the perpendicular field and irradiation dose expressed in terms of the equivalent field $B_\phi = \Phi_0 \phi_t$ for a high-quality Bi 2:2:1:2 single crystal irradiated by 0.5 GeV iodine ions. The dashed line indicates the field above which self-field effects are important (courtesy H.W. Neumüller, Ref. 20).

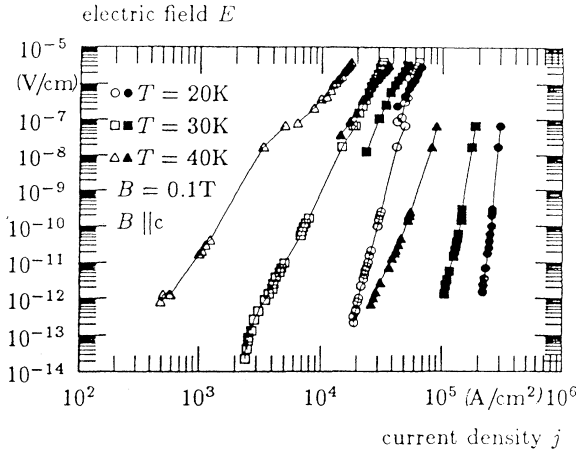

FIG. 9. I-V curves obtained from transport measurements (10^{-7}–10^{-5} V/cm) and magnetization decay (10^{-14}–10^{-7} V/cm) before (open symbols) and after irradiation (solid symbols) with $\phi_t = 2.5 \times 10^{11}$ cm^{-2} ^{127}I (courtesy J.E. Tkaczyk, Ref. 11).

V. CRITICAL CURRENT OF c AXIS WEAK LINKS IN MAGNETIC FIELDS

We consider now the dependence of the critical current across c axis weak links $j_{w,c}$ on field, temperature, and concentration of pinning centers inside the grains.[38,39] The current between two layers labeled by the indices 1 and 2 is given by

$$j_{12}(\rho) = j_{w,c}(0,T)\sin[\varphi_{12}(\rho)], \tag{5.1}$$

$$\varphi_{12}(\rho) = \phi_1(\rho) - \phi_2(\rho) - \frac{2\pi}{\Phi_0}\int_1^2 A_z(\rho,z)dz, \tag{5.2}$$

where $\rho = (x,y)$, and $\phi_{1,2}(\rho)$ are the phases of the order parameter in layers 1 and 2 respectively, $\varphi_{12}(\rho)$ is the gauge-invariant phase difference, and A_z is the c axis component of the vector potential. $j_{w,c}(0,T)$ depends on the value of the order parameter inside the layers. Its dependence on temperature is the same as for standard superconductor-insulator-superconductor (S-I-S) Josephson junctions.[41]

A. Effect of the perpendicular field

We use the Lawrence-Doniach (LD) model[42] to describe the vortex lattice inside the grains. In the presence of a perpendicular field, 2D pancake vortices are nucleated in the CuO_2 layers inside each grain. In this case, the relative positions of the pancake vortices in the top and bottom layers of the grains forming a junction determine the critical current.[38,43] If the pancake vortices in these layers are aligned, the critical current is maximum. If the vortices are misaligned, a phase difference is generated across the junction, and the critical current decreases. Two pancake vortices, one in the top layer

and the other one in the bottom layer of the junction and whose positions are ρ_1 and ρ_2, respectively, induce a phase difference

$$\varphi(x,y) = \arctan\frac{x-x_1}{y-y_1} - \arctan\frac{x-x_2}{y-y_2}\,, \tag{5.3}$$

if we neglect the screening produced by the Josephson current. The two terms in the right-hand side of Eq. (5.3) are the phases produced by the 2D vortices inside the corresponding layers. They coincide with the polar angle around the center of a vortex. For aligned vortices ($\rho_1 = \rho_2$) the phase difference vanishes. For a system of perpendicular vortices with pancakes at positions $\rho_{\mathbf{m},1}$ ($\rho_{\mathbf{m},2}$) in layer 1 (2) the phase difference is

$$\varphi_{12}(\rho) = \sum_{\mathbf{m}} \arctan\frac{x-x_{\mathbf{m},1}}{y-y_{\mathbf{m},1}} - \arctan\frac{x-x_{\mathbf{m},2}}{y-y_{\mathbf{m},2}}\,, \tag{5.4}$$

where $\mathbf{m}$ is a set of two indices labeling the pancake vortices in a given layer. The two-dimensional expression (5.4) is valid at distances smaller than $\hat{\lambda}_J$ from the centers of vortices. At larger distances the interlayer Josephson current is important and decreases the phase difference. Here $\hat{\lambda}_J$ is the Josephson length for the junction between the grains,

$$\hat{\lambda}_J^2 = \frac{c\Phi_0}{16\pi^2 \hat{j}_{0,c}(0,T)\lambda_{ab}}, \tag{5.5}$$

if $\lambda_{ab} > D$; otherwise λ_{ab} should be replaced by D.

The misalignment of the pancake vortices can be caused by pinning or by thermal disorder. In both cases the total maximum current across the junction is given by the following expression:

$$I_{12} = j_{w,c}(0,T)\left|\int d\rho \langle \exp[i\varphi(\rho)]\rangle\right|. \tag{5.6}$$

Here $\langle\cdots\rangle$ denotes either thermal averaging

$$\langle A\rangle = \frac{\int \mathcal{D}\rho_{n,\mathbf{m}} A\{\rho_{n,\mathbf{m}}\}\exp(-\beta\mathcal{F}\{\rho_{n,\mathbf{m}}\})}{\int \mathcal{D}\rho_{n,\mathbf{m}}\exp(-\beta\mathcal{F}\{\rho_{n,\mathbf{m}}\})}\,, \tag{5.7}$$

where $\mathcal{F}\{\rho_{n,\mathbf{m}}\}$ is the free energy functional of the distorted lattice, or impurity averaging, or both depending on the temperature regime and the presence or absence of pinning sites.[44] Well above the irreversibility line, the main effect is the thermally induced disorder, whereas at low temperature pinning-induced disorder represents the main effect.

First, we consider the low field regime (below the depinning line) taking into account the distortions caused by strong pinning inside grains 1 and 2 (as far as pinning-induced disorder is concerned, only plastic distortions of the flux lattice caused by strong pinning centers suppress the critical current).[39] Due to the presence of the pinning centers the positions of the pancake vortices vary from one grain to the next. At a c axis twist boundary the vortex lines jump from one arrangement in the top grain to another in the bottom grain (forming a piece of Josephson vortex between two adjacent layers); see Fig. 10. The shift of the pancake vortices along a vortex line going through a c axis boundary $\mathbf{u_m} = \rho_{\mathbf{m},1} - \rho_{\mathbf{m},2}$ is random. We suppose that the concentration of defects is much larger than the concentration of vortices so that each pancake is shifted from its position in the ideal lattice and these shifts are weakly correlated. The average displacement of a pancake vortex from its ideal equilibrium position in the absence of pinning cannot exceed the intervortex distance $l = \sqrt{\Phi_0/B}$. In the following we assume that the statistical distribution of $\mathbf{u_m}$ is a Gaussian with a standard deviation of order l:

$$p(\mathbf{u_m}) = \frac{b}{\pi l^2}\exp\left(-\frac{bu_{\mathbf{m}}^2}{l^2}\right), \tag{5.8}$$

where b depends on the strength of disorder and is of order unity for strong disorder. The result for the intergrain Josephson critical current is

$$j_{w,c}(B,T)/j_{w,c}(0,T) = \int d\rho \int \mathcal{D}\mathbf{u_m} p(\mathbf{u_m}) \exp\left[i\sum_{\mathbf{m}} \mathbf{D}(\rho-\rho_{\mathbf{m}})\mathbf{u_m}\right] \Big/ \int d\rho, \tag{5.9}$$

where we expand the phase difference in $\mathbf{u_m}$:

$$\varphi(\rho) = \sum_{\mathbf{m}} \mathbf{D}(\rho-\rho_{\mathbf{m}})\mathbf{u_m}, \quad D(\rho) = \left(\frac{y}{\rho^2}, -\frac{x}{\rho^2}\right). \tag{5.10}$$

The sum over m is logarithmically divergent. Upon replacing the summation by an integral we take the size of the unit cell l as the lower integration limit. The upper limit for the summation over the positions of the vortices $\mathbf{m}$ is determined by L if $L < \hat{\lambda}_J$ or by $\hat{\lambda}_J$ if $\hat{\lambda}_J < L$. After performing the integration over $\mathbf{m}$, we get for $L < \hat{\lambda}_J$

$$j_{w,c}(B,T) = j_{w,c}(0,T)(B_0/B)^{\nu}, \tag{5.11}$$

where $B_0 = \Phi_0/L^2$ and $\nu = \pi/4b$. When $L > \hat{\lambda}_J$ the critical current $j_{w,c}(B,T)$ should be determined self-consistently because $\hat{\lambda}_J$ depends on $j_{w,c}(B,T)$; see Ref. 39 for more details. Finally we obtain Eq. (5.11) with $\nu = \pi/(4b-\pi)$ and $B_0 = 16\pi^2 D j_{w,c}(0,T)/c$ assuming $D > \lambda_{ab}$.

In the high field regime pinning can be ignored and

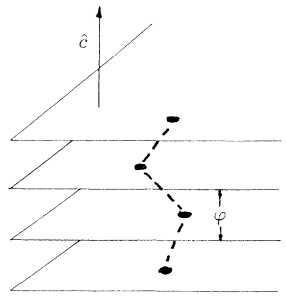

FIG. 10. Distortion of a vortex in a c axis junction responsible for the suppression of the critical current.

only thermal fluctuations should be taken into account. In order to evaluate the critical current, Eqs. (5.6) and (5.7), we use the harmonic approximation for the free energy of the distorted lattice inside the grains and account only for electromagnetic interaction of pancakes, which is correct in the case of strongly anisotropic Bi compounds (for more details see Refs. 38 and 39). The result is

$$j_c(B,T) = j_c(0,T)\exp[-B/B_w(T)], \tag{5.12}$$

$$B_w(T) = \frac{s\Phi_0^3}{32\pi^3 T\lambda_{ab}^4(T)}\frac{\ln(K_0 s)}{\ln[L^{-1}\lambda_{ab}(T)]}, \tag{5.13}$$

where $K_0^2 = 4\pi B/\Phi_0$, s is the interlayer distance, and $\lambda_{ab}(T)$ is the London penetration length which characterizes the electromagnetic coupling of pancakes. The critical current decreases exponentially with field, and the decay constant in the exponential depends strongly on temperature because of the $\lambda_{ab}^4(T)$ factor. The exponential decrease is caused by the thermal fluctuations of the vortices, and the argument of the exponential is proportional to the concentration of vortices, and the mean square distortion $\langle \mathbf{u}_\mathbf{m}^2 \rangle$ which determines the temperature dependence.[40] When $L > \hat{\lambda}_J$ the current decreases almost exponentially until the decoupling field $B_D(T)$ which practically coincides with $B_w(T)$, and the decay constant is practically the same as in Eq. (5.13). Above $B_D(T)$ the critical current vanishes; see Refs. 38 and 39 for more details.

B. Magnetic field parallel to the tape

The effect of a component of the field parallel to the ab plane was discussed in Ref. 10. Now we should also take into account the perpendicular component which is caused by the misalignment of the grains. The component $B_\parallel$ parallel to the y axis generates a phase difference across the junction which is linear in x; the perpendicular component $B_\perp$ generates a phase difference given by Eq. (5.4). The current across the junction is

$$j_{12}(\rho) = j_{w,c}(0,T)\sin\left[\frac{2\pi B_\parallel x\Lambda}{\Phi_0} + \varphi_{12}(\rho)\right], \tag{5.14}$$

where Λ is the effective thickness of the junction. For weak fields $B_\perp$, Λ is given by the standard expression $\Lambda = d + 2\min(\lambda_{ab}, D)$. Here λ_{ab} (or D) is the thickness of the region near the grain where the screening Meissner current flows. The Meissner currents on each side of a junction flow in opposite directions; these currents are very effectively suppressed by the penetration of vortices inside the grains. The presence of vortices decrease the region near the grain surface where the Meissner currents flow.[10,45] More precisely, at $D > \lambda_{ab}$,

$$\Lambda(B_\perp) = d + 2\lambda_{ab}\tanh\frac{z_f(B_\perp)}{\lambda_{ab}}, \tag{5.15}$$

where the thickness of the vortex-free region z_f can be expressed via the magnetization of a grain $M(B_\perp)$:

$$z_f = \lambda_{ab}\left[\frac{8\pi|M(B_\perp)|}{B_\perp}\right]^{1/2}, \tag{5.16}$$

and $|M(B_\perp)| \ll B_\perp$ for $B_\perp \gg H_{c1,\perp}$. In these large fields, $\Lambda \approx d$.

The parallel component of the field determines the Fraunhofer dependence of $j_{w,c}$ on $B_\parallel$ in the absence of the difference of phase φ_{12}. The scale of the field for the Fraunhofer patterns is given by Φ_0/Ld. The disorder in $j_{w,c}(0,T)$ and the random positions of the vortices result in the initial decay of the critical current on this scale (which is not seen experimentally because of the self-field effect). The following decay is determined mainly by the distortions of vortices created by the perpendicular component $B_\perp$; i.e., the critical current is given by Eq. (5.11) where $B = B_\perp$ with $B_\perp$ caused by the misalignment of the grains.

C. Effect of irradiation

The effect of pinning centers on the critical current at low fields or low temperatures was discussed above. Pinning centers lead to a power law dependence of j_c on B, Eq. (5.11). The degree of disorder enters via the parameter b which characterizes the distribution of the pancake vortices deviations across a c axis boundary. We assume that b increases after irradiation by high-energy heavy ions that produce columnar defects. This is because the columns are not perfect throughout the entire sample, and also because the pancake vortices forming a flux line are not necessarily aligned perfectly along the columns in Bi compounds. At $B < B_\phi$, when going from one layer to the next, the pancake vortices adapt to the strongest pinning centers inside the layer rather than always following the column. Therefore we describe the effect of irradiation by means of one parameter $b(\phi_t)$, assuming that it increases with the irradiation dose ϕ_t. If this is the case, the power law dependence of the critical current on B remains valid after irradiation, with the exponent ν increasing with ϕ_t.

In the high magnetic fields regime at moderate and high temperatures strong columnar defects reduce the thermal fluctuations of pancakes. Assuming that each pancake sits in a potential well (at $B < B_\phi$) with radius R_c, the free energy in the harmonic approximation is

$$\mathcal{F}\{\mathbf{u}_{n,\mathbf{m}}\} = \frac{\eta\Phi_0^2 s}{16\pi^2\lambda_{ab}^2}\frac{\mathbf{u}_{n,\mathbf{m}}^2}{R_c^2}, \tag{5.17}$$

where η is a numerical coefficient, $\eta < 1$, and we neglect the interaction of the vortices between themselves. Using Eq. (5.9), we obtain the following expression for B_w:

$$B_{w,c}(T) = \frac{\eta\Phi_0^3 s}{16\pi^2 T\lambda_{ab}^2 R_c^2}\ln\left(\frac{\eta\Phi_0^2 sL^2}{16\pi^2 T\lambda_{ab}^2 R_c^2}\right). \tag{5.18}$$

As a result, the slope of the exponential decay decreases after irradiation because $R_c \ll \lambda_{ab}$. So columnar defects reduce the critical current in the low field regime but they can improve the critical current in the high field regime (at moderate and high temperatures) by suppressing the thermal fluctuations of the vortices. Strong random pointlike pinning centers should suppress the critical current at all fields.

To summarize, in the brick-wall model with c axis

Josephson junctions we have the following behavior of the critical current.

(1) In the low field regime, j_c has a power law dependence on $B_\perp$.

(2) In the high field regime j_c depends exponentially on $B_\perp$. Note that it is the same dependence as for the intragranular pinning mechanism.

(3) The critical current in the low magnetic field regime can decrease after irradiation where column defects are produced. In the high magnetic field regime an increase should be observed.

VI. CRITICAL CURRENT OF *a* AND *b* AXIS WEAK LINKS

The geometry of a and b axis junctions is illustrated in Fig. 11. In perpendicular fields, pancake vortices are nucleated in the CuO_2 layers on each side of a junction. If these vortices are arranged in a regular, periodic manner along the junction, the resulting phase difference across the junction is exactly zero, but if pinning or thermally induced disorder disturbs their equilibrium positions, a phase difference is generated that decreases the critical current. A similar situation was considered recently by Fistul,[46] namely, ordinary Abrikosov vortices parallel to a single Josephson junction. Only pinning-induced disorder was considered.

The phase difference across the junction in the presence of a perpendicular field is

$$\varphi(x) = \varphi_F(x) + \varphi_D(x), \quad \varphi_F(x) = 2\pi B x \Lambda/\Phi_0 , \tag{6.1}$$

$$\varphi_D(x) = \sum_m \left(\arctan \frac{x - x_{\mathbf{m}1}}{y_{\mathbf{m}1}} - \arctan \frac{x - x_{\mathbf{m}2}}{y_{\mathbf{m}2}} \right) . \tag{6.2}$$

The junction plane is determined by $y = 0$ and $\rho_{\mathbf{m}1}$, $\rho_{\mathbf{m}2}$ are the positions of the vortices on the left (1) and right (2) sides of the junction. For a perfectly symmetric arrangements of the vortices with respect to $y = 0$, the phase difference φ_D (which describes the effect of disorder) vanishes. The contribution φ_F describes the Fraunhofer effect on the scale of magnetic field $H_0 = \Phi_0/\Lambda L$, where L is the length of the junction in the x direction. In the presence of disorder inside the weak link or in vortex positions the drop of the critical current $j_{w,ab}$ occurs on the scale H_0. At higher fields $j_{0,ab}$ drops due to the contribution φ_D, and for $B > H_0$ the critical current is

$$j_{w,ab}(B,T) = j_{w,ab}(B \approx H_0, T) \left| \int d\rho \langle \exp\left[i\varphi_D(x) \right] \rangle \right| . \tag{6.3}$$

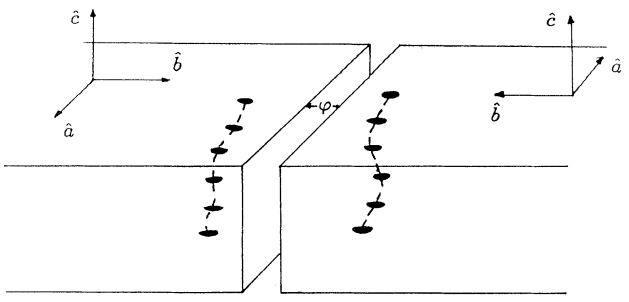

FIG. 11. Geometry of the a and b axis junctions and distortions of vortices in these junctions responsible for the suppression of the critical current.

At low temperatures, the disorder due to pinning is important, and we use Eqs. (5.8)–(5.10) with $\mathbf{u_m} = \mathbf{u_{m1}} - \mathbf{u_{m2}}$. If we assume again a Gaussian distribution for the uncorrelated distortions $\mathbf{u_{m1}}$ and $\mathbf{u_{m2}}$, we obtain the same power law dependence of $\langle \exp(i\varphi_D) \rangle$ on B as given by Eq. (5.11). At high temperatures, the calculations are again similar to those described in the preceding section provided the substitution $\mathbf{u}_m = \mathbf{u}_{m1} - \mathbf{u_{m2}}$ is made. As a result, the dependence $j_{w,ab}$ on B, T is ultimately similar to that given by Eqs. (5.12) and (5.13) with $j_{w,c}(0,T)$ replaced by $j_{w,ab}(B \approx H_0, T)$. Thus the behavior of a and b axis weak links in a perpendicular magnetic field is similar to that of c axis junctions except the initial drop at $B \approx H_0$.

When the field is parallel to the tape, the component of the field along the c axis of the grains is important. Again, this is because of the misalignment of the grains. The Fraunhofer effect associated with the applied field is absent when the field is parallel to the current. When the field is perpendicular to the current the scale of the Fraunhofer effect is now quite large, Φ_0/dD (we replaced Λ by the junction thickness d because of the very small magnetization inside the grains when the field is parallel to the tape, and $B_\parallel \gg H_{c1,\parallel}$). The effect of the parallel component can be neglected in comparison with the effect of the perpendicular component.

Note that the dependence of $j_{w,ab}$ on perpendicular field obtained above can be checked experimentally using bicrystal grain boundary junctions made of Bi- and Tl-based compounds.[47,48]

In conclusion, a magnetic field decreases the critical current of a and b axis weak links much in the same way that it affects the critical current of c axis weak links. Thus, the contribution of a and b axis weak links in the tapes can be accounted for by the renormalization of the parameter $j_{w,c}$.

VII. DISCUSSION OF THE EXPERIMENTAL DATA

We now proceed to a brief description of typical results from I-V curves as well as magnetization and transport critical current measurements in tapes.

A. *I-V* curves

The I-V curves show unambiguously whether the weak links limit the critical current: At $j = j_{w,c}L/D + j_{w,ab}$ a change in the slope of the I-V curves occurs; see Fig. 7. Until recently,[11,27] I-V curves in tapes were not widely available. Hergt *et al.* obtained I-V curves for Bi 2:2:2:3 powder-in-tube samples from magnetization decay at 77 K for small perpendicular fields $B < 88$ mT in the

range 10^{-13} V/cm$< E < 10^{-8}$ V/cm, i.e., below E_c; see Fig. 12. These curves appear as straight lines on a double logarithmic plot. The saturation of the weak links between the short bricks is not seen in the interval of current densities explored in their study. Extrapolation of these curves to $E = E_c$ leads to a critical current at $B \to 0$ of about 7×10^3 A/cm^2 which is a typical value for Bi 2:2:2:3 tapes; see Fig. 13. In the best Bi 2:2:2:3 films this value is about 50 times larger.[37] This means that weak links with $j_1 < 10^2$ A/cm^2 and/or nonsuperconducting phases limit the critical current of the short bricks.

Information on the behavior of the I-V curve in the interval 10^{-8} V/cm$< E < 10^{-4}$ V/cm in the fields 0.1 T and 1 T was obtained by Tkaczyk *et al.*;[11] see Fig. 14. In both fields the power law dependence (3.4) below and above $E_c = 1$ μV/cm was observed. It means that the case "partial limitation by weak links" [shown in Fig. 2(b)] is realized in the tapes studied. Tkaczyk *et al.*[11] came to a similar conclusion. In the field 0.1 T at 77 K $j_c = 2 \times 10^3$ A/cm^2 is about 25 times smaller than in the best film Bi 2:2:2:3 studied by Yamasaki *et al.*[37] This gives upper limit 0.04 for a.

B. Field and temperature dependence of the critical current

The critical current in Bi tapes and in textured polycrystalline thick films of Tl 2:2:1:2, exhibits the following characteristic magnetic field and temperature dependence.[12,11,13,20,49,50]

(1) At low and moderate temperatures ($T \leq 80$ K) and low fields ($B < B_{cr}$), the transport and magnetization critical currents can be described by a power law dependence on the applied magnetic field:

$$j_c(B) = C(T)B^{-\nu}, \tag{7.1}$$

where the temperature independent exponent $\nu \approx 0.45$ for the data in Ref. 12 and 0.3 for the data in Ref. 11. $C = 2 \times 10^4$ AT$^\nu$/cm^2 at $T = 10$ K in both cases. At high fields from about 3 T up to 25 T the critical current is practically field independent.[51]

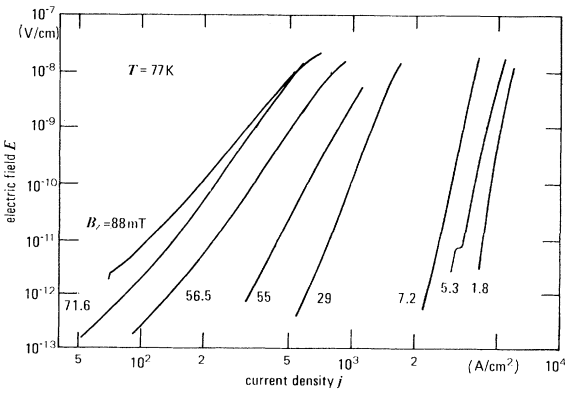

FIG. 12. I-V curves from magnetization decay in Bi 2:2:2:3 powder-in-tube sample (courtesy H.W. Neumüller and M. Leghissa, Refs. 27 and 28).

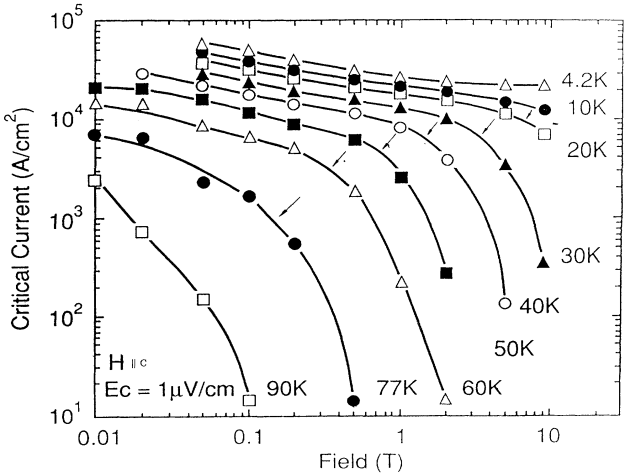

FIG. 13. Temperature and field dependence of the transport critical current in a Bi 2:2:2:3 tape (Ref. 12) for $B \parallel \hat{c}$.

(2) Above B_{cr} the critical current decreases exponentially with the applied magnetic field:

$$j_c(B,T) = j_c(0,T)\exp[-B/B_c(T)], \tag{7.2}$$

and $B_c(T)$ decreases rapidly with increasing temperature. The crossover field B_{cr} also decreases with temperature. The typical magnetic field and temperature dependence of the critical current is shown in Fig. 13. The low-temperature behavior is shown in Fig. 15, and the crossover from the power law dependence of $j_c(B)$ on B to the exponential dependence above B_{cr} is clearly seen in Fig. 16. $B_{cr}(T)$ is indicated by arrows in Fig. 16.

These results are consistent with either "partial limitation by weak links" or "limitation by weak links." If we assume that the latter situation applies, the critical

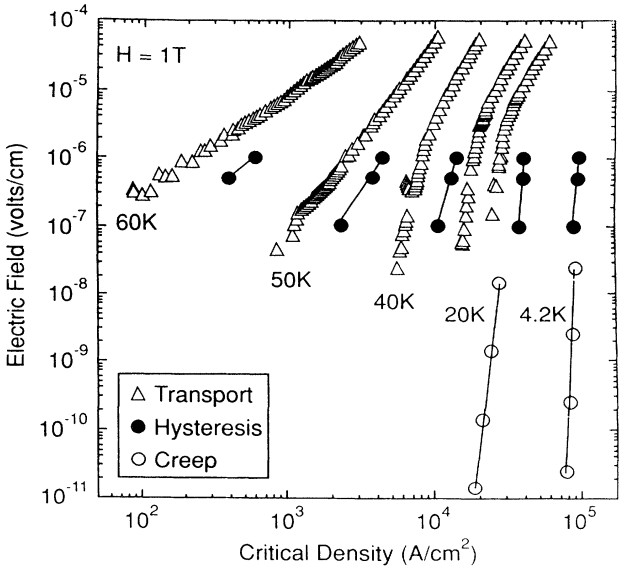

FIG. 14. The electric field versus current density curves obtained from transport, hysteresis, and creep measurements at $B = 1$ T are compared at several temperatures (courtesy J.E. Tkaczyk, Ref. 11).

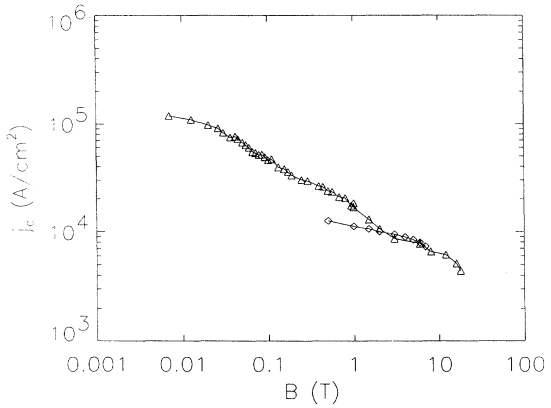

FIG. 15. Magnetic field dependence of the critical current in a Bi 2:2:2:3 tape (triangles, Ref. 12) and a Bi 2:2:1:2 film (diamonds, Ref. 50) for $B \parallel \hat{c}$ at 20 K.

current is limited by the critical current of weak links between the long bricks j_2. In Sec. IV we have shown that in low fields j_2 has a power law dependence on $B_\perp$. At higher magnetic fields j_2 depends exponentially on $B_\perp$. The decay constant $1/B_w(T)$ given by Eq. (5.13) coincides approximately with the experimental data if we take into account the strong dependence of B_w on λ_{ab} and some degree of uncertainty in the extraction of λ_{ab} from experimental data.[52] Upon using Eq. (5.13) for $T = 64$ K and taking $\lambda_{ab}(0) = 2000$ Å, $s = 18$ Å, $L = 20$ μm we estimate the slope in the dependence $\ln j_c$ vs B to be about 5 T^{-1} while the experimental value is about 2 times smaller.[12,20] In a "partial limitation by weak links" scenario, the critical current is aj_p with j_p given by Eq. (4.1) at high magnetic fields. The constant $1/B_p$ is not known in tapes (in high-quality Bi 2:2:2:3 films it is about 20 T^{-1};[37] in tapes it should be smaller because of stronger pinning). Hence, we cannot conclude which case (partial limitation by weak links or limitation by weak links) best explains the dependence of j_c on $B_\perp$.

C. Irradiation effects

Irradiation by 0.65 GeV ^{58}Ni ions with doses of up to 7.7×10^{12} cm^{-2} was used by Neumüller *et al.* to produce columnar defect perpendicular to the tape.[20] They found the following.

(1) The transport critical current at low fields becomes smaller (about 20% for a dose of 7.7×10^{12} cm^{-2}) after irradiation, while at higher fields the critical current increases; see Fig. 17. Notice that in single crystals an increase of the critical current was observed at all fields.

(2) The crossover field separating these two regimes and defined as the field where the effect of irradiation is nil coincides approximately with the magnetic field B_{cr} where the power law dependence of the critical current on magnetic field is replaced by an exponential dependence.

(3) For fields above B_{cr} the critical current depends exponentially on the applied magnetic field (as in unirradiated samples) but the decay constant in the exponential is approximately 2–3 times smaller compared to the unirradiated sample; see Fig. 17.

Similar results were obtained by Civale *et al.*[53] for Bi 2:2:2:3 tapes and by Tkaczyk *et al.*[54] after heavy-ion irradiation of textured $TlSr_2Ca_2Cu_3O_{10}$ (Tl 1:2:2:3) thick films. The decrease of the critical current in zero applied field was a factor of 2 at $\phi_t = 2.4\times10^{11}$ cm^{-2}. The value B_{cr} (1 T at 77 K) determined as the point where the effect of the irradiation on j_c is nil coincides again with the crossover from a power law dependence of $j_c(B)$ to an exponential dependence.

The increase of the critical current at high fields following heavy-ion irradiation can be explained via the mechanisms described by "partial limitation by weak links" or "limitation by weak links." Within the framework of latter case, the increase of the critical current with irradiation at high magnetic fields at moderate and high temperatures can be explained by the suppression of the thermal motion of the pancake vortices aligned inside the columnar defects and the corresponding increase of j_2. If

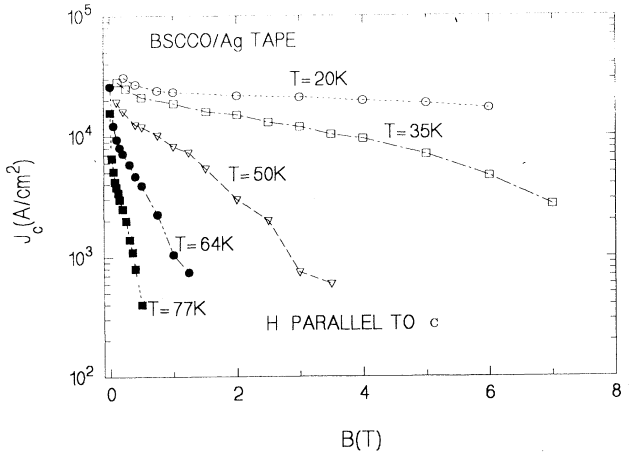

FIG. 16. Temperature and field dependence of the transport critical current in Ag-sheathed Bi 2:2:2:3 tape. The critical current is defined at an electrical field criterion of 1 μV/cm (courtesy J.E. Tkaczyk, Ref. 11).

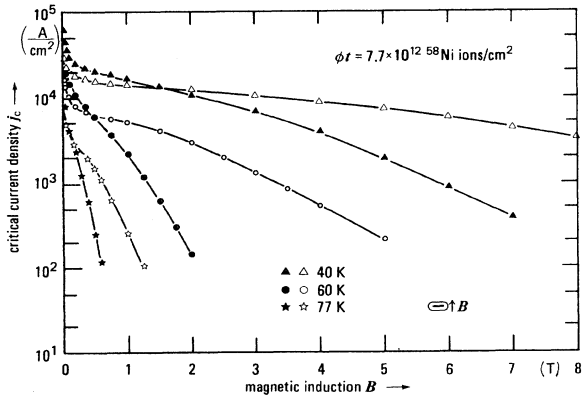

FIG. 17. Field dependence of the transport critical current density of Ag-sheathed Bi 2:2:2:3 tapes before (solid symbols) and after (open symbols) irradiation with 0.65 Gev ^{58}Ni ($\phi_t = 7.7\times10^{12}$ cm^{-2}). $j_{c,t}$ is plotted for $B \perp$ tape (courtesy H.W. Neumüller, Ref. 20).

"partial limitation by weak links" applies, the critical current aj_p increases because of the presence of additional strong pinning centers, namely, columnar defects. The behavior of j_c at high magnetic fields should be the opposite if irradiation produces strong pointlike defects: Either an increase in current will take place due to the enhancement of j_p ("limitation by weak links") or pointlike defects will distort vortices quite effectively at all temperatures and decrease the critical current j_2 ("limitation by weak links").

At low fields the situation is different. If the latter case applies, the suppression of the critical current after irradiation can be explained by the additional deviations of the vortices from a straight lines because the columnar defects are not exactly straight lines themselves (see Sec. V C above).

If "limitation by weak links" applies with $j_c = aj_p$, a decrease of a is possible after irradiation (we further assume that this decrease is not overcome by an increase of j_p as in the high fields).[54] If we denote the volume fraction of the regions where the superconducting phase is destroyed by v, the fraction of the superconducting cross section is $[1-(v/\pi)^{1/2}]$ and $v = \pi R_c^2 \phi_t$. The upper limit for R_c can be obtained by taking into account the fact that the irradiation by heavy ions with $\phi_t = 7.7 \times 10^{12}$ cm^{-2} does not destroy superconductivity.[20] Upon taking the maximum value of v for preserving superconductivity to be 0.5, we obtain $R_c \leq 14$ Å. It follows that at $\phi_t = 3.82 \times 10^{11}$ cm^{-2}, a value used by Tkaczyk *et al.*[54] for irradiation of Tl 1:2:2:3 thick films, the decrease in the superconducting cross section is less than 10% while a decrease in j_c by a factor of approximately 2 was observed. If we take into account that improved pinning should lead to an enhancement of the critical current, we conclude that "partial limitation by weak links" leads to some difficulties in explaining the decrease of the critical current by a factor of 2 in Tl 1:2:2:3 thick films. One can check this conclusion more carefully for tapes and films if the parameter v were known. The fraction of superconducting phase destroyed by irradiation v and the radius of the columns R_c can be obtained from reversible magnetization measurements at high magnetic fields before and after irradiation.

D. Comparison of the critical current in tapes and ground tape powders

Direct information about j_p in tapes comes from the measurements of the irreversible magnetization ΔM in ground tape powder samples. The critical current j_{ps} extracted from such data coincides with j_p if all grains contain superconducting phase at a given temperature. If only part of the tape with fraction f_s is superconducting at given temperature, the measurement of the irreversible magnetization gives $j_{ps} = f_s j_p$ for the powder sample. In the case of "partial limitation by weak links" the ratio of the critical current of the tape j_c and that of the powder sample is $j_c/j_{ps} = a/f_s$.

So far, information about the critical current j_{ps} obtained from irreversible magnetization measurements ΔM in ground tapes is quite limited. Cassidy *et al.*[56] found that the ground tape critical current is larger than that in the tape by one order of magnitude at all temperatures. This is in agreement with the case of "partial limitation by weak links" and gives an upper limit 0.1 for a.

Different results were obtained by Tkaczyk *et al.*:[11] j_{ps} at temperatures below 10 K was found to be about 20 times larger than the tape magnetization critical current and 100 times larger than the transport critical current, while at temperatures above 40 K j_c and j_{ps} practically coincide; see Fig. 18. Based on the low-temperature data, Tkaczyk *et al.* concluded that "partial limitation by weak links" is operative and estimated $a \approx 0.01$ (assuming $f_s = 1$ at low temperatures).

In principle, a strong temperature dependence for the ratio j_c/j_{ps} is possible. The parameter f_s is temperature dependent if tape is made partly of a superconducting phase with lower critical temperature than the Bi 2:2:2:3 phase. Thus results shown in Fig. 18 can be explained by the presence of a lower-T_c phase (presumably Bi 2:2:1:2) in the tape. At low temperatures this phase disconnects grains in the tape, decreasing the critical current, but gives a contribution to the irreversible magnetization of the powder, i.e., $a \ll 1$ and $f_s \approx 1$ at low temperatures. At high temperatures the low-T_c phase again disconnects superconducting grains made of Bi 2:2:2:3 and does not contribute to the irreversible magnetization of powder sample, i.e., $a \ll 1$ and $f_s \approx a$ at high temperatures. It should be mentioned that magnetization measurements probe relaxed current densities that depend upon the time scale of measurement and upon the sample size. Thus, comparisons of results on tapes and powders are expected to diverge at high temperatures, where the powders show stronger relaxation effects due to their smaller size.[57]

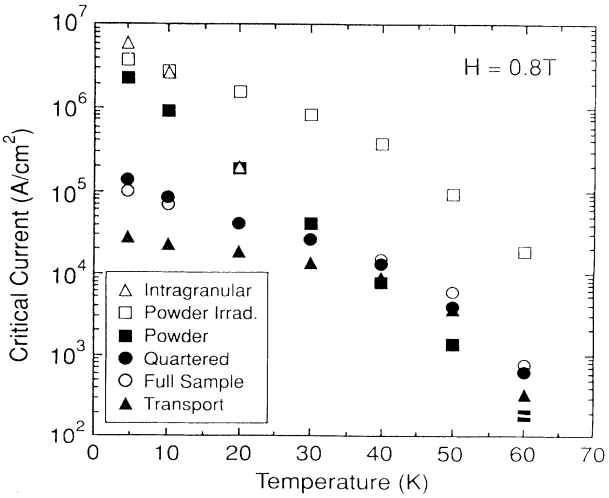

FIG. 18. The critical current versus temperature obtained from transport and magnetization measurements for Bi 2:2:2:3/Ag tapes and magnetization measurements in ground tapes samples. The data for uranium doped Bi 2:2:2:3 powders (Ref. 55) are also plotted (courtesy J.E. Tkaczyk, Ref. 11).

E. Fraction of high-T_c superconducting phase in tapes

Under the condition $j_1 \ll aj_p$, the weakly-coupled short bricks contribute little to the critical current of the tape. From this point of view they are similar to a nonsuperconducting phase (or to a phase with a lower critical temperature, T_{c1} in the temperature range $T_{c1} < T < T_c$). The parameter a then describes the net effect of weakly coupled short grains and of nonsuperconducting phases. In order to separate their contribution, the fraction f_s of superconducting high-T_c phase should be known. The comparison of the critical current in tape and powder discussed above provides some information on f_s. In the following we present an alternative method to determine the fraction f_s of high-T_c Bi 2:2:2:3 phase in the tape.

The parameter f_s can be obtained by measuring, in perpendicular magnetic fields, the magnetic moment $\mathcal{M}(T,B)$ of the tape at temperatures near T_c. In highly anisotropic superconductors such as Bi 2:2:1:2 and Bi 2:2:2:3, at some temperature T^* below T_c, the diamagnetic contribution to the magnetization $M_s(T,B)$ is field independent and $M_s(T^*) = -T^*/\Phi_0 s$, where $s = c/2$ and c is the size of the unit cell along the c axis.[58–61] The curves $\mathcal{M}(B)$ at $T > T_c$ and at $T = T^*$ are parallel to each other, and the volume of high-T_c superconducting phase V_s is given by the expression

$$V_s = [\mathcal{M}(T^*,B) - \mathcal{M}(T > T_c,B)]/M_s(T^*), \qquad (7.3)$$

and $f_s = V_s/V$, where V is the volume of the sample.

The measurements of magnetic moment at $T = T^*$ were performed by Li *et al.*[62] in thin Bi 2:2:2:3 tape characterized by quite high critical current density 3×10^4 A/cm^2 at 77 K in zero field. The parameter f_s extracted from these measurements is only 0.6.

VIII. CONCLUSIONS

The experimental data on I-V curves currently available for tapes[11] shows that the case of "partial limitation by weak links" is realized in high-J_c tapes for $B \leq 1.0$ T. The other more numerous experimental data on the field and temperature dependence of the tape critical current are inconclusive to show that this case is universal for recent tapes.

It seems however that partial limitation of the critical current by weak links (or by nonsuperconducting phases) is at work in any case (it certainly works also in the tape for which I-V curves were obtained[27]). If so, at high temperatures, the parameter a, the fraction of short (weakly coupled) bricks and nonsuperconducting phases, is the main characteristic of the tape. Its optimization implies predominantly the enhancement of the fraction of strongly coupled Bi 2:2:2:3 grains. By optimizing a, it should be possible to increase the critical current by at least one order of magnitude. If the strongly coupled Bi 2:2:2:3 grains are forming near the Ag sheath, then a multilayer structure might prove optimum. The thickness of the BSCCO layer can be made about 10 times smaller than in the most recently fabricated tapes.

The fraction of high-T_c superconducting phase f_s seems to be a very important parameter to increase a because nonsuperconducting phases between superconducting grains disconnect them almost completely. We mentioned above that for the high-quality tape studied by Li *et al.*[62] the parameter f_s is only 0.6. A low fraction of Bi 2:2:2:3 phase may be the main reason for very low values of the parameter a. The temperature dependence of j_c/j_{ps} obtained by Tkaczyk *et al.*[11] and discussed above is in favor of such a conclusion. In addition, Umezawa *et al.*[9] have shown that at 77 K the critical current decreases strongly with increasing concentration of unreacted Bi 2:2:1:2. They concluded that high critical currents can be obtained provided that the Bi 2:2:1:2 fraction is kept low. It seems that a substantial increase of f_s is possible and can be very effective for the improvement of the critical current.

The dependence of the critical current on texture may be quite important also if texture determines the fraction of well-coupled grains, i.e., the value of the parameter a. We mentioned above that the alignment of the grains is about 10° in some of the most recently fabricated tapes. However, the critical current $j_{w,c}$ may not depend on the alignment angle (as was found by Hu *et al.*[19]) The value $j_{w,c}$ depends on the relative orientation of the neighboring grains, being larger for a smoother change of grains orientation along the tape.

In the case of "partial limitation by weak links," i.e., if the long bricks remain connected up to j_c, another important parameter of the tape at moderate and high temperatures is the slope $1/B_p(T)$ in the exponential dependence of $j_p(T)$ on magnetic field. This parameter depends on the strength of the pinning. It is several times smaller in tapes[12,20] compared to the best films.[37] We mentioned above that columnar defects decrease this parameter by a factor of 2 only.[20] It seems that additional possibilities to decrease this parameter in the Bi 2:2:2:3 tapes are very limited because a large number of defects are already introduced during the fabrication process. The replacement of Bi 2:2:2:3 by a less anisotropic superconductor could improve j_p, but enhancement of a seems to be more realistic and more effective at intermediate temperatures and fields. At 77 K, j_p will remain a fundamental limitation for the achievement of higher operating current densities.

In conclusion, the high density current in recent tapes is provided by small fraction a of strongly coupled Bi 2:2:2:3 grains. This fraction can be estimated roughly as $a \leq 0.05$. The other nonworking part of the tape consists of very weakly coupled grains and/or nonsuperconducting phases including phases with lower critical temperature such as Bi 2:2:1:2. It is difficult at this moment to determine what part of the tape is at work; presumably it is a quite thin layer near the Ag sheath (though colony boundaries are candidates as well or strong links for current may be formed randomly). It is also difficult to determine the reason why the main part of the tape is not contributing; one reason is incomplete transformation of the original Bi 2:2:1:2 phase into a high-T_c Bi 2:2:2:3 phase. We wish to emphasize that direct information about the parameters of the tape which control

the critical current may come from the measurements of I-V curves, a comparison of the magnetization critical current $j_{ps}(B,T)$ in ground tapes samples with the magnetization critical current $j_c(B,T)$ of identical tapes, and the determination of the fraction of nonsuperconducting phases. So far, this data has been scarce and the parameters controlling the critical current cannot be identified conclusively.

ACKNOWLEDGMENTS

The authors are grateful to N. V. Coppa, S. Doniach, B. I. Ivlev, A. P. Malozemoff, D. E. Peterson, D. S. Phillips, and J. O. Willis for numerous helpful discussions. We thank D. C. Larbalestier, G. Saemann-Ischenko, J. E. Tkaczyk, H. W. Neumüller, and M. Leghissa for permission to use some of their figures and for sending us results prior to publication. This work was supported by the U.S. Department of Energy.

APPENDIX A

The field dependence of the critical current when the field is applied parallel to the tape can be easily explained if we take into account the fact that the grains making up the tape are not perfectly aligned. Therefore, even when the field is parallel to the tape axis, some grains "see" a c axis component of the applied field because their ab plane is not perfectly parallel to the applied field. Following the experimental observation by Kes *et al.*[17] that only the c axis component of the magnetic field seems to affect the critical current in single crystals, we postulate that for a grain tilted by an angle θ with respect to the plane of the tape, the critical current is given by

$$j_c(\phi,\theta,B) = j_{c\perp}(B)\cos(\phi-\theta) \ , \tag{A1}$$

where $j_{c\perp}(B)$ is the critical current when the magnetic field B is applied perpendicular to the tape. ϕ is the angle between the applied field and the normal to the plane of the tape (see Fig. 19). This approach is reasonable at high magnetic fields at moderate and high temperatures where the critical currents decreases exponentially

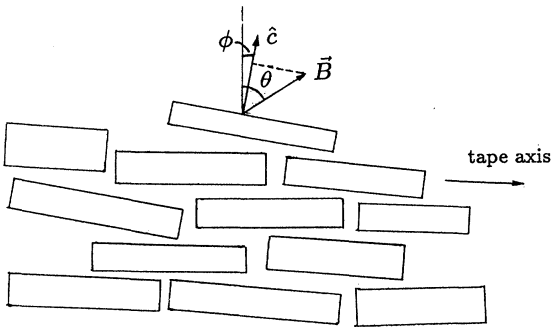

FIG. 19. Misalignment of the grains in a tape.

with perpendicular field. At low temperatures the effect of the parallel component of the field seems to be important, while at higher temperatures it can be neglected in comparison with the effect of the perpendicular component caused by the misalignment of grains.

Next, we assume that the effective critical current density of the tape is obtained by averaging the individual contributions of each grain over the grain orientations. This assumption is valid if the tape is thick enough (compared to the average grain thickness) and/or wide enough (compared to the average grain width). The critical current is then given by the following average:

$$\bar{j}_c(\phi,B) = \int_{-\pi/2}^{\pi/2} d\theta j_{c\perp}[B\cos(\phi-\theta)]p(\theta) \ , \tag{A2}$$

where $p(\theta)$ is the probability distribution of θ. From the above equation, we can obtain the effective critical current density for any orientation of the magnetic field if we assume that (1) $j_{c\perp}(B)$ is known and (2) $p(\theta)$ is known. In the complete absence of detailed information regarding $p(\theta)$, we assume a Gaussian distribution

$$p(\theta) = \frac{1}{\sqrt{2\pi}\sigma}\exp\left(-\frac{\theta^2}{2\sigma^2}\right) \ . \tag{A3}$$

The variance σ^2 characterizes the dispersion of the grains misorientations (θ angle) about an average value that was taken equal to zero here. In the following we assume $\sigma \ll \pi/2$. Upon using Eqs. (A2) and (A3), we obtain

$$\bar{j}_c(\phi,B) = \frac{1}{B\sigma\sin\phi}\int_0^\infty \frac{dx}{\sqrt{2\pi}} j_{c\perp}(x)\left\{\exp\left[-\frac{(x-B\cos\phi)^2}{2B^2\sigma^2\sin^2\phi}\right] + \exp\left[-\frac{(x+B\cos\phi)^2}{2B^2\sigma^2\sin^2\phi}\right]\right\} \ . \tag{A4}$$

From experimental data for $j_{c\perp}(B)$, we can extract the parameter σ by fitting the effective critical current obtained from Eq. (A4) with $\phi = \pi/2$ to the experimental curve, $j_c(B_\parallel)$. The result of such a fit is shown in Fig. 20 for two temperatures. The theoretical expression reproduces the experimental result remarkably well for $\sigma \simeq 16°$. (Notice that the two fits for $T = 64$ K and $T = 75$ K lead to the same value for σ—a good indication that σ is indeed related directly to the microstructural properties of the tape.) A similar value for σ was reported by Hu *et al.*[19] from critical current measurements and also by Wilhelm *et al.*[63] from a SEM observation of a Bi 2:2:2:3 tape. We can test Eq. (A2) over the entire angular range available for ϕ. The result is shown in Fig. 21 for an applied field intensity of 0.25 T at $T = 64$ K.

APPENDIX B

In order to estimate the effect of the self-field on the transport critical current, consider a tape of thickness D_t, width $2W_t$, and length L_t. Usually $D_t \ll W_t$, and we

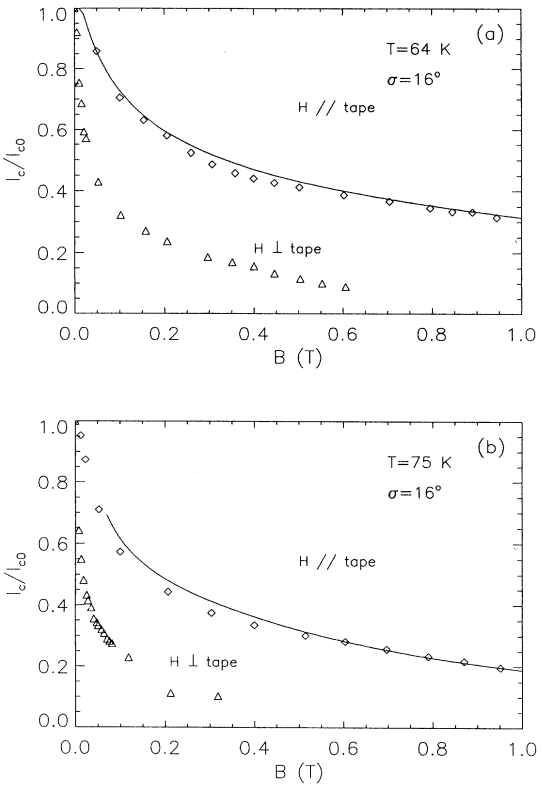

FIG. 20. Magnetic field dependence of $j_{c,t}$ when the field is perpendicular (triangles) and parallel (diamonds) to a Bi 2:2:2:3 tape. The fit was obtained from Eq. (A4). (a) $T = 64$ K, (b) $T = 75$ K.

can replace the tape by an infinitely thin current sheet. If $j_y(x)$ designates the critical current density at x (x axis is along the tape perpendicular to the current, y axis is along the tape and along the current, z axis is perpendicular to the tape) the equation for the vector potential is

$$-\nabla^2 A_y(x,z) = \frac{4\pi}{c} j_y(x) D_t \delta(z) \ . \tag{B1}$$

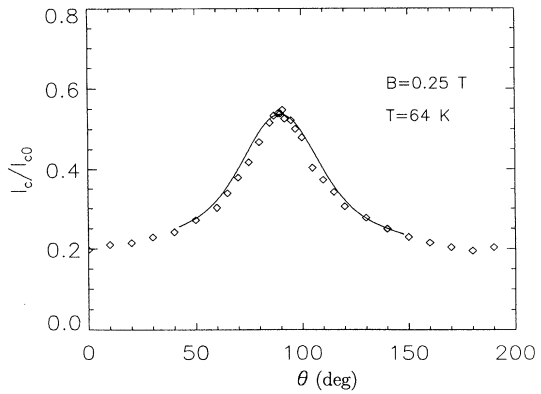

FIG. 21. Dependence of $j_{c,t}$ on the angle between the applied field and the normal to the plane of the tape for a Bi 2:2:2:3 tape. The fit was obtained from Eq. (A2).

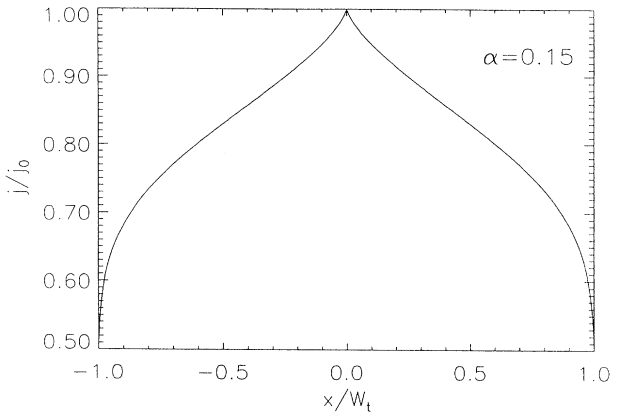

FIG. 22. Depression of the critical current density in a tape due to the self-field effect. The x axis is perpendicular to the current in the plane of the tape; W_t is the width of the tape.

From the solution of this equation, one gets the z component of the magnetic field:

$$B_z(x, z=0) = \frac{2D_t i}{c} \int_{-\infty}^{+\infty} dk \int_{-W_t}^{W_t} j_y(x') \exp[-ik(x'-x)] \mathrm{sgn}(k) \ . \tag{B2}$$

We ignore the parallel component of the magnetic field because the effect of the z component is much stronger. If we consider the high-temperature regime and assume an exponential dependence of the critical current on the perpendicular component of the magnetic field,

$$\frac{j(x)}{j_0} = \exp[- \mid B_z(x) \mid / B_c] \ , \tag{B3}$$

we get the following integral equation for the critical current:

$$\ln \frac{j(x)}{j_0} = -\alpha \left| P \int_{-W_t}^{W_t} dx' \, \frac{j(x')/j_0}{x'-x} \right| \ , \tag{B4}$$

where $\alpha = 4D_t j_0 / cB_c$ and P indicates that the Cauchy principal value of the integral should be considered. We solve the above equation after substituting typical values for the various parameters: $j_0 \approx 10^5$ A/cm^2, $D_t \approx 200$ μm, and $B_c \approx 0.5$ T, which correspond to $\alpha = 0.15$. The total suppression of the current by self-field effects is determined by the value of

$$\beta = \frac{1}{2W_t} \int \frac{j(x)}{j_0} dx < 1 \ . \tag{B5}$$

For the above parameters, we found $\beta = 0.82$, which is not a very large reduction. Notice however that the critical current is significantly suppressed (by a factor of 2 approximately) at the edges of the tape, Fig. 22. This is simply due to the fact that the self-field is maximum at the edges whereas it vanishes in the middle by symmetry.

Note that the effect of the self-field is more important at low temperatures where $j_{0,c}$ depends strongly on B in the limit of small B; see Eq. (5.11).

[1]K. Sato, T. Hikata, H. Mukai, T. Masuda, M. Ueyama, H. Hitotsuyanagi, T. Mitsui, and M. Kawashima, in *Advances in Superconductivity II*, edited by T. Ishiguro and K. Kajimura (Springer-Verlag, Tokyo, 1990), p. 335; T. Hikata, M. Ueyama, H. Mukai, and K. Sato, Cryogenics **30**, 924 (1990); K. Sato, T. Hikata, H. Mukai, M. Ueyama, N. Shibuta, T. Kato, T. Masuda, M. Nagata, K. Iwata, and T. Mitsui, IEEE Trans. Magn. **MAG-27**, 1231 (1991).

[2]J. Mannhart, in *Earlier and Recent Aspects of Superconductivity*, edited by J.G. Bednorz and K.A. Müller, Springer Series in Solid-State Sciences Vol. 90 (Springer-Verlag, Berlin, 1990), p. 208; J. Mannhart and C.C. Tsuei, Z. Phys. B **77**, 53 (1989).

[3]A.P. Malozemoff, *Superconductivity and its Applications*, AIP Conf. Proc. No. 251, edited by Y.H. Kao *et al.* (American Institute of Physics, New York, 1992), p. 6.

[4]Y. Feng, K.E. Hautanen, Y.E. High, D.C. Larbalestier, R. Ray II, E.E. Hellstrom, and S.E. Babcock, Physica C **192**, 293 (1992).

[5]Y. Feng, Y.E. High, D.C. Larbalestier, Y.S. Sung, and E.E. Hellstrom, Appl. Phys. Lett. **62**, 1553, 1993.

[6]B. Hensel, J.C. Grivel, A. Jeremie, A. Perin, A. Pollini, and R. Flükiger, Physica C **205**, 329 (1993).

[7]The condition for the Josephson interlayer coupling is $\xi_z \ll s$, where ξ_z is the superconducting correlation length along c axis and s is the interlayer spacing. This condition can be rewritten in the form $(T_c - T)/T_c \gg \xi_{ab}^2(0)/\gamma^2 s^2$ where $\xi_{ab}(T)$ is the correlation length in the ab plane and γ is the anisotropy ratio. For Bi compounds $\xi_{ab}(0) \approx 25$ Å and $s = 15$ Å for Bi 2:2:1:2 and 18 Å for Bi 2:2:2:3. The anisotropy ratio for Bi 2:2:2:3 is about 30 according to H_{c2} measurements near T_c; see I. Matsubara, H. Tanigawa, T. Ogura, H. Yamashita, and M. Kinoshita, Phys. Rev. B **45**, 7414 (1992). This value is probably a lower limit for γ. For Bi 2:2:1:2 a lower limit for the anisotropy ratio at high temperatures seems to be about 200; see J.C. Martinez, S.H. Brongersma, A. Koshelev, B. Ivlev, P.H. Kes, R.P. Griessen, D.G. de Groot, Z. Tarnavski, and A.A. Menovsky, Phys. Rev. Lett. **69**, 2276 (1992) and Y. Iye, I. Oguro, T. Tamegai, W.R. Datars, N. Motohira, and K. Kitazawa, Physica C **199**, 154 (1992). Therefore, the Josephson regime is important practically at all temperatures below T_c in the Bi compounds.

[8]It is also possible that impurities present during the fabrication process tend to concentrate preferentially along a and b axis boundaries outside of colony boundaries, further weakening those weak links.

[9]A. Umezawa, Y. Feng, H.S. Edelman, D.C. Larbalestier, Y.S. Sung, E.E. Hellstrom, and S. Fleshler, Physica C **198**, 261 (1992).

[10]L.N. Bulaevskii, J.R. Clem, L.I. Glazman, and A.P. Malozemoff, Phys. Rev. B **45**, 2545 (1992).

[11]J.E. Tkaczyk, R.H. Arendt, M.F. Garbauskas, H.R. Hart, K.W. Lay, and F.E. Luborsky, Phys. Rev. B **45**, 12 506 (1992).

[12]M.P. Maley, P.J. Kung, J.Y. Coulter, W.L. Carter, G.N. Riley, and M.E. McHenry, Phys. Rev. B **45**, 7566 (1992).

[13]H.K. Liu, Y.C. Guo, S.X. Dou, S.M. Cassidy, L.F. Cohen, G.K. Parkins, A.D. Caplin, and N. Savvides (unpublished).

[14]R.L. Peterson and J.W. Ekin, Phys. Rev. B **37**, 9848 (1988).

[15]J.W. Ekin, T.M. Larson, A.M. Hermann, Z.Z. Sheng, K. Togano, and H. Kumakura, Physica C **160**, 489 (1989).

[16]D.P. Hampshire, X. Cai, J. Seuntens, and D.C. Larbalestier, Supercond. Sci. Technol. **1**, 12 (1988).

[17]P.H. Kes, J. Aarts, V.M. Vinokur, and C.J. van der Beck, Phys. Rev. Lett. **64**, 1063 (1990).

[18]P. Schmitt, P. Kummeth, L. Schultz, and G. Saemann-Ischenko, Phys. Rev. Lett. **67**, 267 (1991).

[19]Q.Y. Hu, H.W. Weber, S.X. Dou, H.K. Liu, and H.W. Neumüller (unpublished).

[20]H.W. Neumüller, W. Gerhäuser, G. Ries, P. Kummeth, W. Schmidt, S. Klaumünzer, and G. Saemann-Ischenko, Phys. Rev. Lett. **68**, 879 (1992).

[21]P. Schmitt, L. Schultz, and G. Saemann-Ischenko, Physica C **168**, 475 (1990).

[22]V.M. Vinokur, M.V. Feigel'man, and V.B. Geshkebein, Phys. Rev. Lett. **67**, 915 (1991).

[23]M.V. Feigel'man, V.B. Geshkebein, A.I. Larkin, and V.M. Vinokur, Phys. Rev. Lett. **63**, 2303 (1989).

[24]Y. Yeshurun and A.P. Malozemoff, Phys. Rev. Lett. 60, 2202 (1988).

[25]M. Tinkham, Phys. Rev. Lett. **61**, 1658 (1988).

[26]E. Zeldov, N.M. Amer, G. Koren, and A. Gupta, Appl. Phys. Lett. **56**, 1700 (1990).

[27]R. Hergt, R. Hiergeist, J. Taubert, H.W. Neumüller, and G. Ries, Phys. Rev. B **47**, 5405 (1993).

[28]G. Ries, H.W. Neumüller, R. Busch, P. Kummeth, M. Leghissa, P. Schmitt, and G. Saemann-Ischenko, Alloys Compounds **195**, 379 (1993).

[29]E.H. Brandt, Phys. Rev. B **46**, 8628 (1992).

[30]J.R. Thompson, Y.R. Sun, H.R. Kerchner, D.K. Christen, B.C. Sales, B.C. Chakoumakos, A.D. Marwick, L. Civale, and J.O. Thompson, Appl. Phys. Lett. **60**, 2306 (1992).

[31]L. Klein, E.R. Yacoby, Y. Yeshurun, M. Konczykowski, F. Holtzberg, and K. Kishio, Physica C **209**, 251 (1993).

[32]R.C. Budhani, M. Suenaga, and S.H. Liou, Phys. Rev. Lett. **60**, 3816 (1992).

[33]P. Kummeth, H.W. Neumüller, G. Ries, M. Kraus, S. Klaumünzer, and G. Saemann-Ischenko, J. Alloys Compounds **195**, 403 (1993).

[34]J.R. Clem, Phys. Rev. B **43**, 7837 (1991).

[35]The pinning energy of a single pancake vortex by a columnar defect can be estimated as the core energy of a 2D vortex. This energy is $\approx \Phi_0^2 s/16\pi^2\lambda_{ab}^2$, where λ_{ab} is the penetration depth for the current along the ab plane. For $s = 18$ Å, $\lambda_{ab} = 2000$ Å we obtain an energy close to 70 meV.

[36]We note that in tapes a and b axis weak links and secondary phase boundaries are equivalent to columnar defects from the point of view of pinning because the superconducting order parameter is strongly reduced inside these boundaries. However, the concentration of such defects is quite small in comparison to the number of intragranular defects. For this reason it is probably reasonable to neglect the effect of these defects. In fact, the influence of grain boundaries on the critical current was not found in the case of textured Bi 2:2:1:2 bulk samples as compared with epitaxial films; see Ref. 18.

[37]H. Yamasaki, K. Endo, Y. Nakagawa, M. Umeda, S. Kosaka, S. Misawa, S. Yoshida, and K. Kajimura, J. Appl. Phys. **72**, 2951 (1992); H. Yamasaki, K. Endo, S. Kosaka, M. Umeda, S. Yoshida, and K. Kajimura, Phys. Rev. Lett. **70**, 3331 (1993).

[38]L.L. Daemen, L.N. Bulaevskii, M.P. Maley, and J.Y. Coulter, Phys. Rev. Lett. **70**, 1167 (1993).

[39]L.L. Daemen, L.N. Bulaevskii, M.P. Maley, and J.Y. Coul-

ter, Phys. Rev. B **47**, 11 291 (1993).

[40]Note that we calculated the thermodynamical critical current which can be probed by static measurements. In the presense of transport current through the junction at nonzero temperature the voltage should appear at any current due to vortex fluctuations. For finite junction without vortices similar effect was calculated by Ambegaokar and Halperin; see V. Ambegaokar and B.I. Halperin, Phys. Rev. Lett. **22**, 1346 (1969).

[41]A. Barone, *Physics and Applications of the Josephson Effect* (Wiley, New York, 1984).

[42]W.E. Lawrence and S. Doniach, in *Proceedings of the 12th International Conference on Low Temperature Physics, Kyoto 1970,* edited by E. Kanda (Keigaku, Tokyo, 1970).

[43]S.L. Miller, K.R. Biagi, J.R. Clem, and D.K. Finnemore, Phys. Rev. B **31**, 2684 (1985).

[44]The thermal averaging of the current is an exact procedure. In the case of disorder caused by pinning centers, the average current may not be very significant if the current fluctuations are large. The latter are certainly important when the average current becomes very small, as in the case for the Fraunhofer dependence of the critical current on a magnetic field parallel to the junction; see I.K. Yanson, Zh. Eksp. Teor. Fiz. **58**, 1497 (1970) [Sov. Phys. JETP **31**, 800 (1970)]. Here we consider only the case of a sufficiently large critical current so that the effect of fluctuations can be ignored. This approximation is correct because many uncorrelated weak links contribute to the total current.

[45]J.R. Clem, in *Low Temperature Physics—LT 13*, edited by K.D. Timmerhaus, W.J. O'Sullivand, and E.F. Hammel (Plenum Press, New York, 1974), Vol. 3, p. 102.

[46]M.V. Fistul, Pis'ma Zh. Eksp. Teor. Fiz. **52**, 823 (1990) [JETP Lett. **52**, 192 (1990)].

[47]A.H. Cardona, H. Suzuki, T. Yamashita, K.H. Young, and L.C. Bourne, Appl. Phys. Lett. **62**, 411 (1993).

[48]M. Kawasaki, E. Sarnelli, P. Chauhari, A. Gupta, A. Kussmaul, J. Lacey, and W. Lee, Appl. Phys. Lett. **62**, 417 (1993).

[49]M.P. Maley, G.J. Vogt, D.S. Phillips, J.Y. Coulter, P.N. Arendt, and N.E. Elliot, IEEE Trans. Magn. **MAG-27**, 1139 (1991).

[50]S. Labdi, H. Raffy, O. Laborde, and P. Monceau, Physica C **197**, 274 (1992).

[51]N. Shibuta, M. Ueyama, H. Mukai, and K. Sato, Jpn. J. Appl. Phys. **30**, L2083 (1991).

[52]For Bi 2:2:2:3 from the magnetization data at high temperatures the value $\lambda_{ab}(0) = 2320$ Å was obtained by A. Schilling, F. Hulliger, and H.R. Ott, Z. Phys. B **82**, 9 (1992). The account of the vortex fluctuations should make this value smaller; see V.G. Kogan, M. Ledvij, A.Yu. Simonov, J.H. Cho, and D.C. Johnston, Phys. Rev. Lett. **70**, 1870 (1993).

[53]L. Civale, A.D. Marwick, R. Wheeler, M.A. Kirk, W.L. Carter, G.N. Riley, Jr., and A.P. Malozemoff, Physica C **208**, 137 (1993).

[54]J.E. Tkaczyk, J.A. DeLuca, P.L. Karas, P.J. Bednarczyk, D.K. Christen, C.E. Klabunde, and H.R. Kerchner, Appl. Phys. Lett. **62**, 3031 (1993).

[55]H.R. Hart, F.E. Luborsky, R.H. Luborsky, R.H. Arendt, R.L. Fleischer, J.R. Tkaczyk, and D.A. Orsini, IEEE Trans. Magn. **MAG-27**, 1375 (1991).

[56]A.D. Caplin, S.M. Cassidy, L.F. Cohen, M.N. Cuthbert, J.R. Laverty, G.K. Perkins, S.X. Dou, Y.C. Guo, H.K. Liu, H.J. Tao, and E.L. Wolf, Physica C **209**, 167 (1993).

[57]M.V. Feigel'man, V.B. Geshkebein, and V.M. Vinokur, Phys. Rev. B **43**, 6263 (1991).

[58]P.H. Kes, C.J. Van der Beck, M.P. Maley, M.E. McHenry, D.A. Huse, M.J.V. Menken, and A.A. Menovsky, Phys. Rev. Lett. **67**, 2383 (1991).

[59]L.N. Bulaevskii, M. Ledvij, and V.G. Kogan, Phys. Rev. Lett. **68**, 3773 (1992).

[60]Z. Tešanović, L. Xing, L. Bulaevskii, Q. Li, and M. Suenaga, Phys. Rev. Lett. **69**, 3563 (1992).

[61]F. Zuo, D. Vacaru, H.M. Duan, and A.M. Hermann, Phys. Rev. B **47**, 8327 (1993).

[62]Q. Li, M. Suenaga, T. Hikata, and K. Sato, Phys. Rev. B **46**, 5857 (1992).

[63]M. Wilhelm, H.W. Neumüller, and G. Ries, Physica C **185-189**, 2399 (1991).

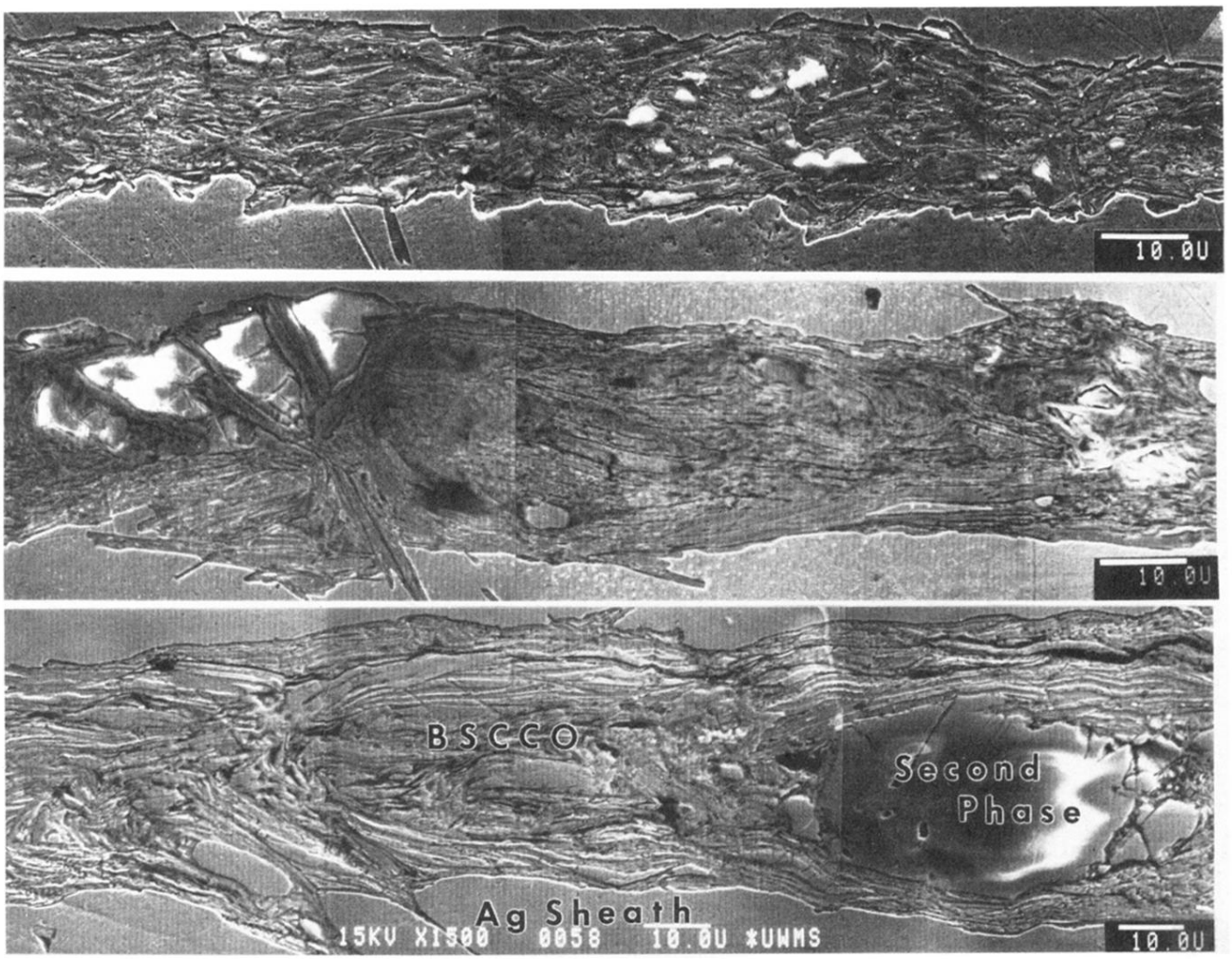

FIG. 1. Scanning electron microscope (SEM) micrographs of polished and etched thin-longitudinal cross-section samples: (a) solid state, (b) fast-cooled, and (c) slow cooled. The local grain alignment interrupted by second-phase particles can be seen clearly (courtesy Yvonne High, Ref. 4).

FIG. 3. Transmission electron microscope (TEM) micrography of a thin-longitudinal cross section of a fast-cooled sample showing an overview of the grain morphology and grain boundaries (beam direction perpendicular to the c axis of Bi 2:2:1:2). The colony boundaries are indicated (courtesy Yi Feng, Ref. 4).

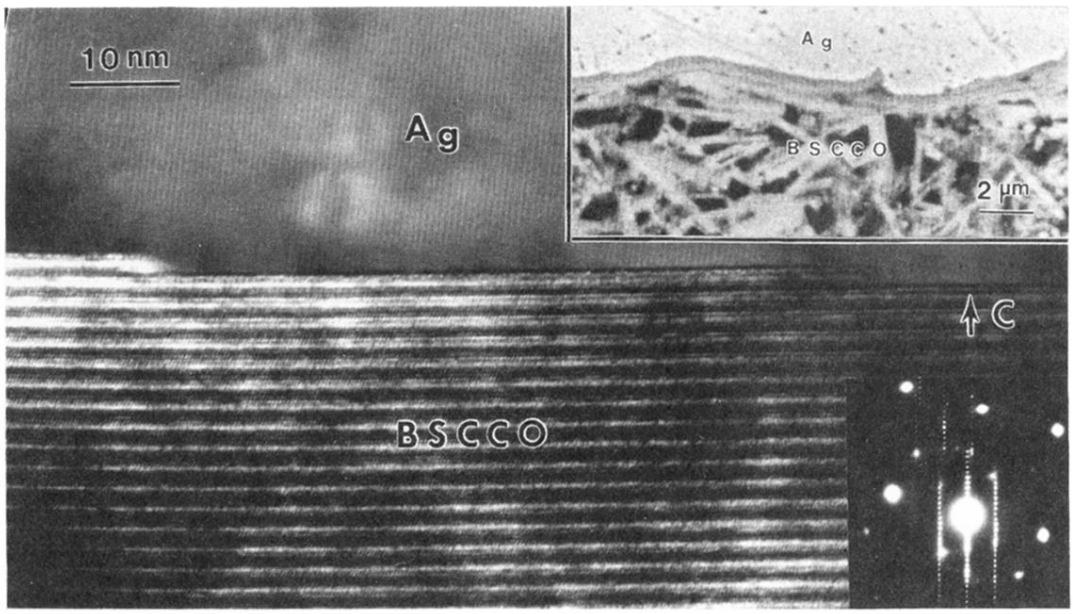

FIG. 4. TEM (001) lattice fringe image of the Bi 2:2:1:2 phase in the slow-cooled sample showing its c axis perpendicular to the interface with the Ag cladding. The inset is a SEM micrography of a transverse cross section of the same tape (courtesy Yi Feng, Ref. 5).

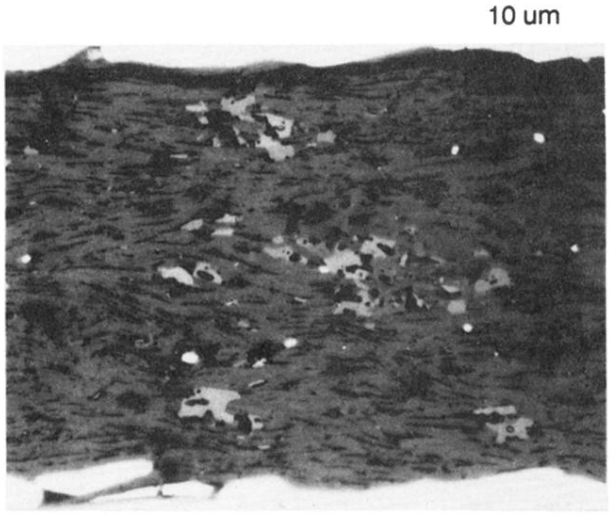

FIG. 5. Optical reflection in polished, rolled, sintered Bi 2:2:2:3 tape. Gray regions are Bi 2:2:2:3 grains, black regions are epaxi, which is used to fill empty space in between grains before polishing, and white regions are secondary phases.